Title
Two Models of Self-Interacting Dark Matter

Permalink
https://escholarship.org/uc/item/0930q561

Author
Smolenski, Sarah Elizabeth

Publication Date
2019

Peer reviewed|Thesis/dissertation

UNIVERSITY OF CALIFORNIA
RIVERSIDE

Two Models of Self-Interacting Dark Matter

A Dissertation submitted in partial satisfaction
of the requirements for the degree of

Doctor of Philosophy

in

Physics

by

Sarah Smolenski

June 2019

Dissertation Committee:

    Dr. Jose Wudka, Chairperson
    Dr. Haibo Yu
    Dr. Owen Long

The Dissertation of Sarah Smolenski is approved:

_____

_____

_____
Committee Chairperson

University of California, Riverside

Acknowledgments

Many thanks to my advisor, without whom I would never have made it this far.

To my family for everything they gave.

ABSTRACT OF THE DISSERTATION

Two Models of Self-Interacting Dark Matter

by

Sarah Smolenski

Doctor of Philosophy, Graduate Program in Physics
University of California, Riverside, June 2019
Dr. Jose Wudka, Chairperson

I explore two possible extensions to the standard model. The first is a simple addition, including only one additional scalar particle with an exact $U(1)$ symmetry, which allows the dark boson to condense even when relativistic. The second model includes five new fields consisting of: two dark matter candidates; a mediator boson; heavy dark neutrinos; and a heavy scalar.

Contents

List of Figures

Chapter 1

Introduction

1.1 Background

1.1.1 Motivation

In 1933, Fritz Zwicky noted [30] an inconsistency between observations of galaxy motion across the sky by Van Maanen [20] and Hubble's determination of the distance to same galaxies [12]. When Zwicky used these values to calculate the total velocity of various galaxies, he found unexpectedly large speeds. When he compared these speeds to those calculated via the Virial theorem, he found that his calculated velocities were several orders of magnitude larger than those allowed by energy considerations, assuming that all mass in the galaxy cluster was made up of luminous matter. On the other hand, if the average density of the Coma cluster was 400 times[1] greater than observed then the expected galaxy velocities would be possible. This is largely regarded as the first experimental evidence for

---

[1]Zwicky's estimation of the density of the cluster is over by roughly an order of magnitude due to his use of the then-modern measurement value of the Hubble Parameter, which differs from today's value by roughly one order of magnitude.

dark matter.

In the decades since Zwicky's paper was published, we have collected a myriad of evidence, all of which suggest that the universe contains several times more matter than is visible or predicted by the Standard Model. Though Zwicky's analysis of the Coma cluster was the first, other clusters followed rapidly and all exhibited the same high-velocity behavior [28]. Spectra analysis of the Andromeda galaxy [1] revealed that the stars far from the center were also moving with a much higher rotational velocity than should have been possible from visible matter alone, which was later extended to even greater radii to the same effect [25, 23]. This later analysis provides some of the most well-known evidence for the theory of dark matter 1.1. Given that the majority of luminous matter lies within 10 kpc radii, rotational velocity was expected to drop off as $v_{rot} \sim \sqrt{\frac{GM}{R}}$. Instead, no drop-off was observed, and it appeared instead that the mass of most, if not all, galaxies increased steadily with increasing radius [9].

Other observational evidence for the existence of missing matter came in the form of X-ray emissions of early galaxies [4], which were observed to have luminous coronae explainable by massive halos, and gravitational lensing around the bullet cluster [21], which showed the gravitational mass distribution from two merging clusters distinct from their luminous mass distribution (fig. 1.2). While other theories have attempted to explain one or many of the discrepancies between Newtonian gravity and observation, none describe all of the evidence so neatly as the theory of dark matter; that is to say, the theory that out universe contains roughly five times more mass than the visible baryonic matter predicted by our current theories of astroparticle physics.
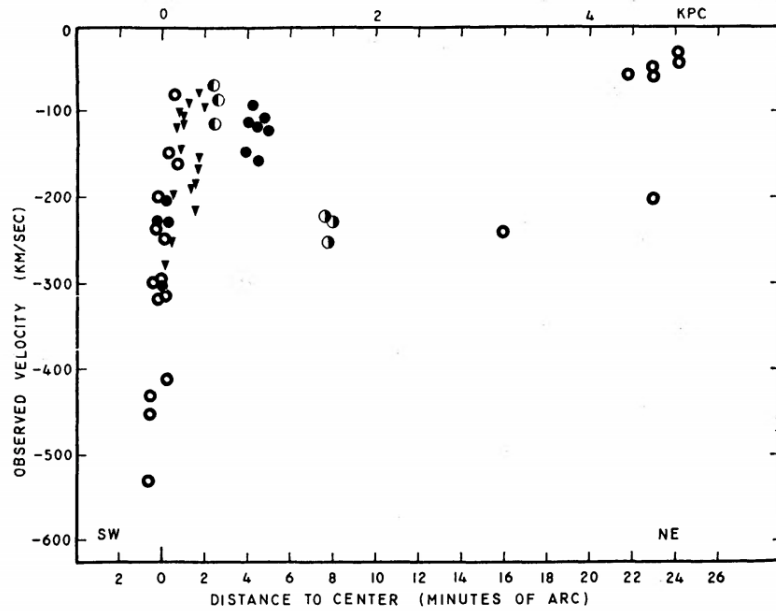
Figure 1.1: Reference [26]. Observed velocity of stars in Andromeda galaxy climbs sharply as expected, but remains roughly constant rather than dropping off, as predicted by Keplerian physics.
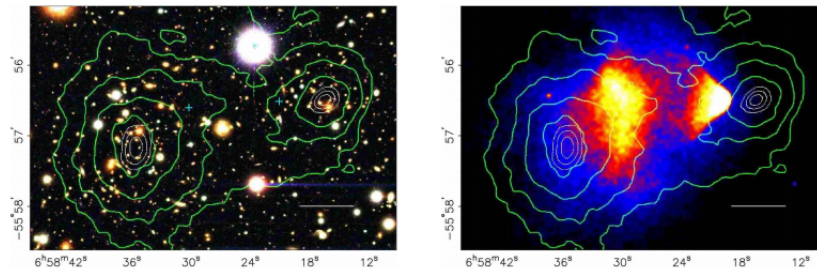
Figure 1.2: While the visible matter is sparse and passes through without collision or apparent interaction, gravitational lensing shows that the majority of the mass contained in the clusters did, in fact, appear to collide and drag behind. The heatmap shows the distribution of the gravitational mass and the green contours show the weak lensing reconstruction.
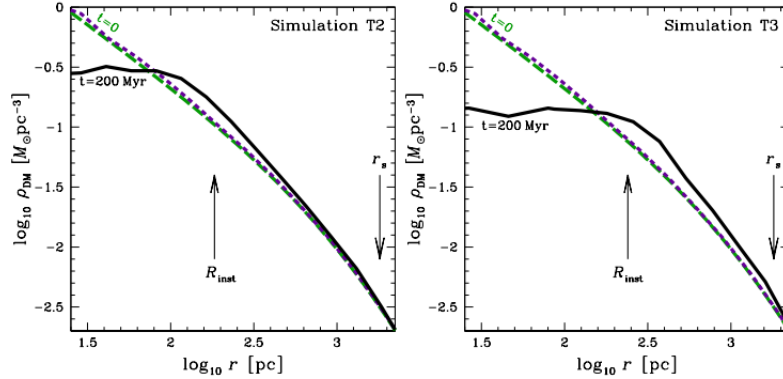
Figure 1.3: Simulations run by Nipoti and Binney. [21] show the flattening of dark matter density profiles over time, as produced by a repulsive self-interaction introduced only between dark matter particles.

1.1.2 Empirical Evidence for Self-Interaction of Dark Matter

While dark matter has long been assumed to be inert, insofar as it does not appear to interact with the Standard Model particles, save through gravity, more recent considerations suggest that dark matter must have some form of self-interaction. If dark matter was subject only to gravitational forces, we would expect to find that the distribution of mass in the dark matter halo was 'cusp-shaped' near the center of the galaxy. That is to say, density of dark matter should rise sharply near to galactic center due to gravitational attraction. We find this is not the case at all. While dark matter density rises near the center of the galaxy, density curves display a flattening or 'core-shaped' behavior close to $r = 0$. This is commonly known as the Core vs Cusp problem. Simulations (fig. 1.3) show that this behavior is achievable by introducing a repulsive force between dark matter particles. Thus, when the density is high enough near the center of the galaxy, this repulsive force is able to balance the gravitational attraction and prevent the cusp-shaped density profile.

1.1.3 The Standard Model

The models proposed in this thesis stand as an extension to the Standard Model (SM) of particle physics. While the SM does an extraordinary job of describing the physics of baryonic matter, it offers no insight into the current mystery of dark matter. Countless possibilities exist for modifications to the SM, but we require that the models discussed herein comply with observables and, in the case where newly-proposed DM particles decay to SM particles or vice versa, that enhancements to decay widths are small enough not to interfere with known values.

The theories discussed below couple to the SM in various ways, and we will use $\mathcal{L}_{SM}$ to denote the standard model lagrangian as given by

$$
\begin{aligned}
\mathcal{L}_{SM} = \ & -\frac{1}{4}B_{\mu\nu}B^{\mu\nu} - \frac{1}{8}tr\left(W_{\mu\nu}W^{\mu\nu}\right) - \frac{1}{2}tr\left(G_{\mu\nu}G^{\mu\nu}\right) \\
& + (D_\mu H)^\dagger D_\mu H - m_H^2 \frac{\left(H^\dagger H - v^2/2\right)^2}{2v^2} \\
& + \left\{ L_L\bar{\sigma}^\mu i D_\mu L_L + e_R^\dagger \sigma^\mu D_\mu e_R - \frac{\sqrt{2}}{v}L_L^\dagger H M_e e_R \right\} + h.c. \\
& + \{Q_L^\dagger \bar{\sigma} i D_\mu Q_L + u_R^\dagger \sigma^\mu i D_\mu u_R + d_R^\dagger \sigma^\mu i D_\mu d_R \\
& - \frac{\sqrt{2}}{v}\left[Q_L^\dagger H M_d d_R + D_L^\dagger \tilde{H} M_u u_R\right]\} + h.c
\end{aligned}
\tag{1.1}
$$

where $B_{\mu\nu}$ is the $U(1)$ hypercharge gauge field, $W_{\mu\nu}$ is the $SU(2)$ isospin gauge field, $G_{\mu\nu}$ is the $SU(3)$ color gauge field, L_L and Q_L denotes the left-handed lepton and quark isodoublets, respectively, and H is the Higgs doublet. This lagrangian can easily be modified to include similar terms for right-handed neutrinos, which have not been observed.

1.2 Introduction

I have studied two different potential models for self-interacting dark matter. The first model is a simplistic model introducing only one new particle to modify the standard model: a massive boson, which couples directly to itself to produce a self-interaction and interacts with the standard model via a Higgs Portal. It should be noted that while we include a self-interaction in this model, we did not consider the constraints on such a coupling that the observed galaxy and cluster density profiles would impose. Thus, while this model has the potential to address the core-vs-cusp problem in future work, we do not consider this here. This bosonic dark matter is unique in that it can form a Bose-Einstein condensate; this condensing potential will affect the dark matter-standard model interaction cross section, regrdless of whether or not a condensate exists in the universe.

The second model I consider here introduces a total of five new fields. The dark matter candidates are two fermions of (approximately) equal mass which have opposite $U(1)_{dark}$ charge. The dark matter particles do not couples directly to the Standard Model. Instead, I include a massive scalar particle which allows the dark matter to interact with the Standard Model via one-loop interactions (to lowest order). Thus, the direct detection cross section will be naturally small without any fine tuning of the coupling constants. In addition to these three fields, I also introduce a dark photon, the $U(1)_{dark}$ vector boson, which mediates the dark matter self-interactions, and three heavy, dark neutrinos, which mix with the Standard Model neutrinos to produce the neutrino-portal coupling. This model includes a (softly broken) dark $\mathbb{Z}_2$ symmetry, which prevents the dark photon from mixing with the Standard Model photon. Strong constraints are placed on this model from

electroweak experiments, but a region of viable parameter space remains to be searched. Furthermore, we consider the limits placed on this model from preventing the two dark matter candidates from forming bound states, but it is worth nothing that these constraints are likely too stringent and a more in-depth study of reasonable limits would benefit the model. We leave these calculations for a later publication.

Chapter 2

Bose-Einstein Self-Interacting Dark Matter

2.1 The Model

We consider a dark matter model that introduces a new (exact) $U(1)$ symmetry under which all standard model particles are singlets. In certain circumstances, this symmetry will allow a Bose-Einstein condensate (BEc) of dark matter (DM) particles to form. This model includes only one new DM particle: a single complex scalar labeled χ, which is invariant under the the transformation:

$$\chi \to e^{i\alpha}\chi, \quad (\alpha = const.) \tag{2.1}$$

which leads to the required conservation law. This exact symmetry means that the presence or absence of a BEc depends entirely on the temperature and density of the gas; that is to

8

say, the condensate in this model is not limited to the non-relativistic regime. The conserved dark charge of χ implies the existence of a non-zero chemical potential $\mu \leq m_\chi$, where the condition $\mu = m_\chi$ implies the existence of a condensate.

A self-interaction of the form $|\chi|^4$ is introduced, which will have an effect on the existence of a condensate in the early universe. The model has the following lagrangian:

$$\mathcal{L} = |\partial\chi|^2 - m_\chi^2|\chi|^2 - \frac{1}{2}\lambda_\chi|\chi|^4 + \epsilon|\chi|^2|\phi|^2 + \mathcal{L}_{SM} \tag{2.2}$$

where ϕ is the standard model scalar isodoublet and $\mathcal{L}_{SM}$ denotes the Standard Model lagrangian. We will consider the mass region $m_\chi \geq 1 GeV$ where the DM is WIMP-like, but we will briefly discuss the region $m_\chi \lesssim 2 \times 10^{-11} eV$ where there will be a BEc in the present epoch.

2.2 Cosmology with a Bose Gas

We model the early universe as containing both SM and DM particles, initially in equilibrium with each other. That is, we assume that the rate of expansion of the universe is sufficiently slow, such that at sufficiently early times both SM and DM gases will be in thermodynamic equilibrium. We assume a flat, homogeneous, and isotropic universe. As the universe cools and expands, decoupling will occur between the SM and DM systems, however, we assume that λ_χ is large enough that the DM remains in thermodynamic equilibrium with itself throughout. For the case where $\lambda_\chi = 0$, the quantities under consideration are simply the well-known expressions for an ideal Bose gas [24]. We assume that λ_χ is small enough that we can describe our system as a perterbative expasion of the ideal gas case. For the discussion

9

below, we will ignore $\mathcal{O}(\epsilon)$ contributions, assuming that ϵ is large enough to have allowed equilibrium between the SM and dark sector in the very early universe, but is otherwise much smaller than the dominant contributions in the range of parameters considered here: $m_{be} \lesssim m_H$ and $|\epsilon| \lesssim \lambda_\chi$.

We write the occupation numbers for χ and anti-χ as

$$n_{be}^+ = \left(e^{(E-\mu)/T} - 1\right)^{-1} = \left(e^{x\left(\sqrt{u^2+1}-\varpi\right)} - 1\right)^{-1}; \quad x = \frac{m_\chi}{T}, \; \varpi = \frac{\mu}{m_\chi} \tag{2.3}$$

$$n_{be}^- = \left(e^{(E+\mu)/T} - 1\right)^{-1} = \left(e^{x\left(\sqrt{u^2+1}+\varpi\right)} - 1\right)^{-1}, \tag{2.4}$$

where $E = \sqrt{\boldsymbol{p}^2 + m_\chi^2}$ and $u = |\boldsymbol{p}|/m_\chi$.

We define

$$\delta = \frac{\mu^2 - m_\chi^2}{\lambda_\chi}, \quad \mathbb{F} = 2 \int \frac{d^3\boldsymbol{p}}{(2\pi)^3 2E} \left[n_{be}^+ + n_{be}^-\right]_{\mu=m_\chi}, \tag{2.5}$$

(see Appendix for further discussion) the phase transition line is given by

$$\delta = \mathbb{F}. \tag{2.6}$$

If $\mu^2 < m_\chi^2 + \lambda_\chi \mathbb{F}$ then no condensate will form. As expected, in the absence of self-interaction (ie, $\lambda_\chi = 0$), this reduces to the well-known result that a condensate will exist if $|\mu| = m_\chi$.

The conserved charge associated with the $U(1)$ symmetry of the model is

$$q_{be} = q_{be}^{(c)} + q_{be}^{(e)} \tag{2.7}$$

10

$$q_{be} = q_{be}^{(c)} + m_{be}^3 \nu_{be}; \quad \nu_{be} = \int_0^\infty \frac{du\, u^2}{2\pi^2} \left(n_{be}^+ - n_{be}^-\right) + \mathcal{O}(\lambda_\chi), \tag{2.8}$$

where $q_{be}^{(c,e)}$ are the charge densities in the condensate and the excited states, respectively. For conveniance we can assume $q_{be}^{(c)} \geq 0$ so that if there is a condensate, μ will be greater than 0.

We write the entropy and energy densities of the Bose gas as

$$s_{be} = m_\chi^3 \sigma_{be}; \quad \sigma_{be} = \int_0^\infty \frac{du\, u^2}{2\pi^2} \sum_{n=n_{be}^\pm} \left[(1+n)\ln(1+n) - n\ln n\right] + \mathcal{O}(\lambda_\chi) \tag{2.9}$$

$$\begin{aligned} \rho_{be} &= q_{be}\mu + T s_{be} - P_{be} \\ &= m_{be}q_{be}^{(c)} + m_{be}^4 r_{be}; \quad r_{be} = \int_0^\infty \frac{du\, u^2}{2\pi^2} \sqrt{u^2+1}\left(n_{be}^+ + n_{be}^-\right) + \mathcal{O}(\lambda_\chi). \end{aligned} \tag{2.10}$$

Though we do not write out the $\mathcal{O}(\lambda_\chi)$ corrections in this section, they are used in the equations below and discussed further in the Appendix.

The corresponding energy and entropy densities from the Standard Model are given by [17]

$$\rho_{sm} = \frac{\pi^2}{30}T^4 g_*(T), \quad s_{sm} = \frac{2\pi^2}{45}T^3 g_*(T), \tag{2.11}$$

where

$$g_*(T) \simeq \sum_{bosons} g_i \left(\frac{T_i}{T}\right)^4 \theta\left(T - m_i\right) + \frac{7}{8}\sum_{fermions} g_i \left(\frac{T_i}{T}\right)^4 \theta(T - m_i), \tag{2.12}$$

11

$$g_{*s}(T) \simeq \sum_{bosons} g_i \left(\frac{T_i}{T}\right)^3 \theta(T - m_i) + \frac{7}{8} \sum_{fermions} g_i \left(\frac{T_i}{T}\right)^3 \theta(T - m_i), \qquad (2.13)$$

where g_i is the number of internal degrees of freedom and T_i is the temperature for each particle.

The Bose Einstein Condensate

When the SM and Bose gas are in equilibrium with each other, q_{be}/s_{tot} is conserved, where $s_{tot} = s_{SM} + s_{be}$. When they are not in equilibrium with each other, q_{be}/s_{SM} and s_{be}/s_{sm} are separately conserved. Thus, regardless of whether they are in equilibrium with each other,

$$Y = \frac{q_{be}}{s_{tot}} \qquad (2.14)$$

is conserved. A condensate will necessarily exist whenever $Y > Y^{(e)}$. That is, whenever the total charge is greater than that contained in the excited states:

$$q_{be}^{(c)} \neq 0 \quad if \quad Y > Y^{(e)} = \frac{\nu_{be}}{\sigma_{be} + s_{sm}/m_{be}^3} |_{\delta=\mathbb{F}}. \qquad (2.15)$$

Since s_{sm} is positive and nonzero, we can write:

$$Y^{(e)} < \left.\frac{\nu_{be}}{\sigma_{be}}\right|_{\delta=\mathbb{F}} < \left.\frac{\nu_{be}}{\sigma_{be}}\right|_{\delta=\mathbb{F},\, T\to 0} = \frac{\zeta_{3/2}}{(5/2)\zeta_{5/2}} \simeq 0.78 \qquad (2.16)$$

Then a condensate will form whenever the total charge is larger than the excited-state charge:

$$Y < Y^{(e)} < 0.78 \qquad\qquad (2.17)$$

Therefore, if $Y > 0.78$ there will always be a condensate. The behavior of $Y^{(e)}$

for different values of λ_χ and m_χ are graphed in (fig. 2.1). We see that in the case of no

self-interaction, (that is, $\lambda_\chi = 0$) at sufficiently early times or, equivalently, at sufficiently

high temperatures there will always be a condensate. However, when $\lambda_\chi \neq 0$, $Y^{(e)}$ has an

m_χ dependent minimum, such that for certain values of Y it is possible that a condensate

will never form, regardless of temperature.

We note that $Y^{(e)}$ decreases for increasing temperature due to the temperature-

density exchange in the early universe. At sufficiently early times (or, equivalently, sufficiently

high temperatures) the density of the DM gas is necessarily high due to the small volume of

the universe. While the high temperature tends to destroy the condensate, the high density

tends to produce it and the volume effect wins out until sufficiently high density is acheived,

at which point the repulsive force from λ_χ dominates and $Y^{(e)}$ begins to increase again.

It is worth noting, though we do not include the calculations here, that the presence

of the chemical potential allows us to determine the relic abundance of the DM. We use this

to fix μ and guarantee that the relic abundance is in agreement with observation without

restricting other parameters.

2.2.1 Conditions for a BEc to exist at present

The Bose gas and SM will decouple at some decoupling temperature, which we

denote T_d. For WIMP-like masses ($m_\chi \gtrsim 1\text{GeV}$), the BE gas will be nonrelivistic at this
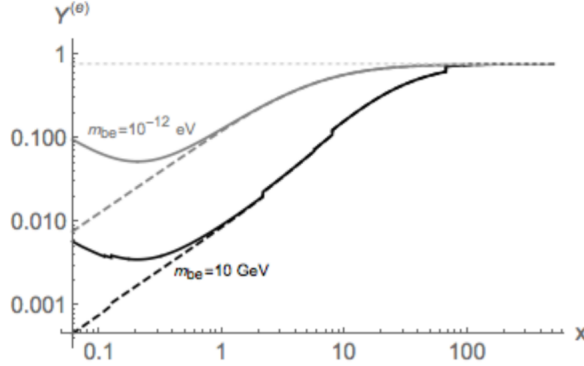
Figure 2.1: Plot of the Bose charge in the excited states per entropy when $\lambda_\chi = 0.5$ (solid curve) and $\lambda_\chi = 0$ (dashed curves) and for two mass values: $m_\chi = 10 GeV$ (black curves) and $m_\chi = 10^{-12} eV$ (grey curves). The horizontal dotted line corresponds to the upper bound. We have assumed the Bose gas and SM have the same temperature. The discontinuities are due to the step functions in eqn. (2.13) and $x = m_\chi/T$.

decoupling temperture; it follows, then, that the gas will be nonrelativistic at present. In the nonrelativistic limit $\mathcal{O}(\lambda_\chi)$ will be smaller than the $\mathcal{O}(T/m_\chi)$ corrections and can be safely ignored (see eqn (A.20) and surrounding discussion in the Appendix). Then, using the measured relic density and standard model entropy, and the fact that q_{be}/s_{sm} is conserved, we have

$$\frac{q_{be}}{s_{sm}} \simeq \frac{1}{m_\chi}\frac{\rho_{DM}}{s_{sm}} = \frac{0.4eV}{m_\chi} \quad (T < T_d), \tag{2.18}$$

where we have included the known value for the SM entropy at present along with $\rho_{DM} = m_\chi q_{be}$. After decoupling (ie $T < T_d$), the left hand side is conserved.

A condensate will be present if

$$\frac{q_{be}(T_d)}{(m_\chi T_d)^{3/2}} > \frac{\zeta_{3/2}}{(2\pi)^{3/2}} \simeq 0.166. \tag{2.19}$$

which implies (using eqns (2.18) and (2.11))

14

$$\frac{T_d^{3/2}}{m_{\chi}^{5/2}} g_{*s}(T_d) > \frac{1}{1.06\text{eV}} \tag{2.20}$$

$$\Rightarrow m_{be} < 1.3\text{keV} \quad (3\sigma) \tag{2.21}$$

where we have used the fact that $m_{be} > T_d$ for a nonrelativistic gas and $g_{*s} < 106.75$.

We now consider the present epoch, denoting the temperture of the BE gas now as T_{now}. From the above, it follows that there will be a condensate in the present if

$$\left(\frac{0.0215\text{eV}}{m_{be}}\right)^{5/3} \text{K} > T_{now} \tag{2.22}$$

The conservations of the quantity s_{be}/s_{now} allows us to obtain a relationship between T_{now} and T_d, the temperature of the BE gas when it decoupled from the standard model. We note, also, that in order for a BEc to exist at present, one must have existed at decoupling. So we have

$$\frac{4.3K}{g_{*s}(T_d)^{1/3}} = \sqrt{T_d T_{now}}, \tag{2.23}$$

where we have used eqn (2.10) and eqn (2.11). Combining this with eqn (2.22) and corrections included in the Appendix,

$$(g_{*s}(T_d)\text{eV})^{2/3} T_d \gtrsim \left(\frac{m_{\chi}}{0.009eV}\right)^{5/3} \text{K}. \tag{2.24}$$

Then, using the fact that $m_{\chi} > T_d$,

$$9.5 g_{*s}(T_d)\text{eV} \gtrsim m_{\chi} \Rightarrow m_{\chi} < 88\text{eV}, \tag{2.25}$$

15

so we find that a WIMP-like DM will be able to maintain a condensate at present, assuming that the gas is uniformly distributed in the universe. However, if one includes the constraints from Big Bang Nucleosynthesis and Large Scale Structure Formation, the constraints on m_χ are much stronger.

2.3 Bose condensate in the small mass region

As noted above, a condensate can occur when the gas has sub-eV masses. In this case, however, there are additional constraints stemming form the possible effects of such light particles on large scale structure (LSS) formation and on big-bang nucleosynthesis (BBN). In this section we will investigate the regions in parameter space allowed by these constraints assuming that the gas is currently condensed; as noted above this ensures the presence of a condensate in earlier times[1].

For the small masses needed to ensure the presence of a BEc now (see below) the condition $H = \Gamma$ would require a coupling ϵ orders of magnitude above the perturbativity limit, hence in this case the gas is decoupled from the SM during the BBN and LSS epochs.

LSS formation occurred at redshift $z_{\mathsf{LSS}} \sim 3400$, when the matter-dominated era began. To ensure that the Bose gas does not interfere with the formation of structure we require it to be non-relativistic at that time; in addition, since we assume the presence of a BEc at present, a BEc was also present at the LSS epoch. Then the conservation of $a^3 s_{be}$ gives, using the appendix, $a^3 x^{-3/2} =$constant (a denotes the scale factor in the Robertson-Walker metric); equivalently,

---

[1]At least as long as $x > \lambda_\chi > 8.8$.
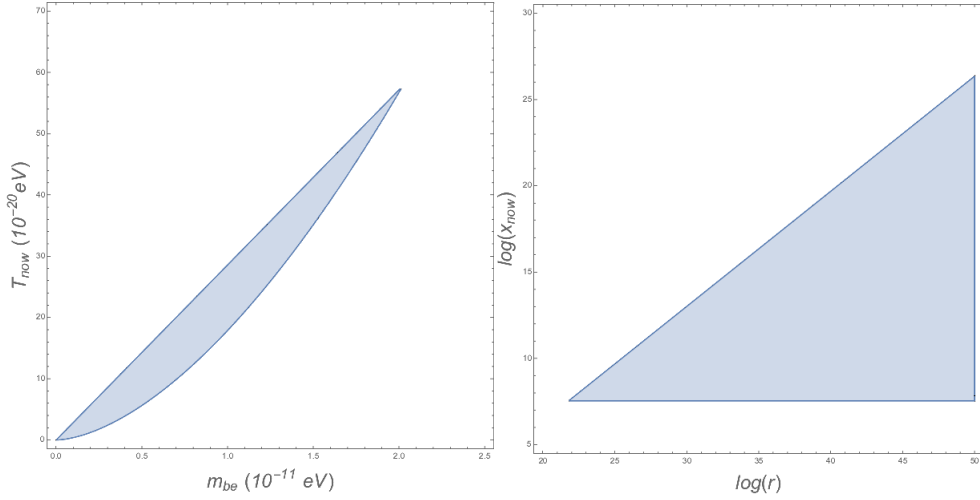
Figure 2.2: Regions of the $m_\chi - T$ and $r - x$ planes where a non-relativistic Bose condensate occurs consistent with the LSS constraint of eqn (2.27. On the left-hand graph the low-T limit results from eqn (2.28, while the upper limit is due to eqn (2.27).

$$\frac{a^2}{x}|_{now} = \frac{a^2}{x}|_{LSS} \tag{2.26}$$

Since the gas must be non-relativistic during the LSS epoch, $x_{\mathsf{LSS}} > 3$, so we have

$$x_{now} > 3.5 \times 10^7 \tag{2.27}$$

In addition, the requirement that a BEc be present now implies

$$\frac{0.4eV}{m_{be}} s_{sm}|_{now} > \left(\frac{m_{be}^2}{2\pi x_{now}}\right)^{3/2} \zeta_{3/2} \tag{2.28}$$

where we used the fact that the gas is currently non-relativistic.

The regions in the $m_\chi - T$ and $m_{chi} - x$ planes allowed by eqns (2.27) and (2.28) are given in Figure 2.2 (here T refers to the gas temperature). It is worth noting that if these conditions occur at present, most of the gas will be in the condensate: using eqns

17

(2.18) and (2.27) the gas fraction in the excited states is given by

$$\frac{q_{be}^{(e)}}{q_{be}}|_{now} < \left(\frac{m_{be}}{1.82eV}\right)^4 , \tag{2.29}$$

which is negligible in view of the range of masses being here considered (see figure 2.2.

We now turn to the BBN constraints. We write the contributions from the gas to the energy density in the form of an effective number of neutrino species ΔN_ν:

$$\rho_{be}|_{\text{BBN}} = \frac{3}{\pi^2}\frac{7}{4}\left(\frac{4}{11}\right)^{4/3}\Delta N_\nu\, T_\gamma^4 \simeq 0.138\Delta N_\nu\, T_\gamma^4 , \tag{2.30}$$

where $T_\gamma \simeq 0.06\,MeV$ denotes the photon temperature during BBN. Imposing the relic-abundance constraint (2.18) we find, using eqns (2.10) and (2.8),

$$\Delta N_\nu = 7.2 \times 10^{-5} + 7.24\frac{m_\chi^4}{T_\gamma^4}\left[r_{be}(x_{\text{BBN}}) - \nu_{be}(x_{\text{BBN}})\right]_{\delta \geq \mathbb{F}} . \tag{2.31}$$

where $r_{be} - \nu_{be}$ corresponds to the energy outside the condensate.

The limit $-0.7 < \Delta N_\nu < 0.4$ shows that the first contribution to ΔN_ν can be ignored. Also, the LSS constraint $m_\chi < 2\times10^{-11}\,eV$ (see Fig. 2.2), implies $(m_\chi/T_\gamma) \lesssim 10^{-62}$, so that the second contribution to ΔN_ν is also small except if the gas was ultra-relativistic during BBN. In this case

$$\Delta N_\nu \simeq 4.76\left(\frac{m_\chi}{T_\gamma x_{\text{BBN}}}\right)^4\left[1 + \frac{5\lambda_\chi}{16\pi^2}\right] , \quad x_{\text{BBN}} \ll 1 , \tag{2.32}$$

so the BBN constraint is significant only in the extreme ultra-relativistic case where $x_{\text{BBN}} < 10^{-62}$.
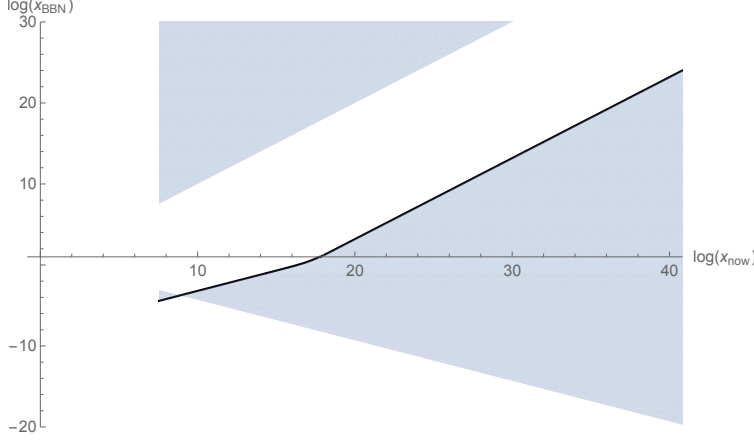
Figure 2.3: Region in the $x_{\text{BBN}} - x_{\text{now}}$ plane consistent with the conservation laws, and with the assumption that a BEc is currently present. We used the expressions in appendix () and $ s_{sm}|_{\text{now}} = 2889.2/cm^3$, $s_{sm}|_{\text{BBN}} = 4.82 \times 10^{28}/cm^3$ and took $\lambda_{chi} = 0.5$. When $\lambda_\chi = 0$ the allowed region collapses to the bold dark line in the figure.

To examine this possibility we first obtain in figure 2.3 the regions in the $ x_{\text{BBN}} - x_{now}$ plane consistent with the fact that s_{be}/s_{sm} and q_{be}/s_{sm} are conserved, together with the assumption that a BEc is currently present. The lower bound in this region corresponds to $x_{\text{BBN}} \geq 4.9/\sqrt{x_{\text{now}}}$; using this, and the BBN constraint $\Delta N_\nu < 0.4$ in eqn (2.32), we obtain

$$x_{\text{now}} < 1.1 \times 10^{125} \left(\frac{m_\chi}{10^{-11} eV} \right)^{-2} \left(1 - \frac{5\lambda_{be}}{32\pi^2} \right) , \qquad (2.33)$$

To understand the gap that appears in figure 2.3 consider the expressions in Appendix: we write $[\lambda_\chi C^2/(sm_\chi^2)]s_{be}^{(c)}$ (this defines $s_{be}^{(e,c)}$) and use $C^2 = [q_{be} - q_{be}^{(e)}]/m_\chi + O(\lambda_\chi) $; then, noting that $s_{be}^{(c)} \gg s_{be}^{(c)} q_{be}^{(c)}$ (which we verified numerically), and using the fact that s_{be}/s_{sm} and q_{be}/s_{sm} are constant, we find

$$\frac{\left[s_{be}^{(e)}/s_{sm} \right]_{\text{BBN}} - \left[s_{be}^{(e)}/s_{sm} \right]_{\text{now}}}{\left[s_{be}^{(c)} \right]_{\text{now}} - \left[s_{be}^{(c)} \right]_{\text{BBN}}} = \frac{\lambda_\chi}{2m_\chi^3} \frac{q_{be}}{s_{sm}} > \frac{\lambda_\chi}{2m_\chi^3} \frac{q_{be}^{(c)} e}{s_{sm}} \Bigg|_{\text{now}} , \qquad (2.34)$$

where the inequality on the right-hand side imposes the constraint that a BEc is

19

present now. The gap in figure 2.3 corresponds to values of $x_{\mathsf{BBN,now}}$ where the denominator and numerator have opposite signs. For example, if the gas is non-relativistic during nucleosynthesis,

$$\frac{1 - \vartheta\,(x_{\mathsf{now}}/x_{\mathsf{BBN}})^{3/2}}{1 - \sqrt{x_{\mathsf{now}}/x_{\mathsf{BBN}}}} > \frac{3\lambda_\chi}{40\pi}\frac{\zeta_{3/2}^2}{\zeta_{5/2}}\frac{1}{2\pi x_{\mathsf{now}}}\,, \quad \vartheta = \frac{s_{sm}|_{\mathsf{now}}}{s_{sm}|_{\mathsf{BBN}}} \simeq 6 \times 10^{-26}\,; \tag{2.35}$$

in this case the gap corresponds to $ \log x_{\mathsf{now}} \gtrsim \log x_{\mathsf{BBN}} \gtrsim -16.8 + \log x_{\mathsf{now}}$.

The parameter region where the gas exhibits a BEc now and satisfies both the LSS and BBN constraints are determined by eqns (2.33), (2.27) and the allowed $x_{\mathsf{BBN}} - x_{\mathsf{now}}$ and $m_\chi - T_{\mathsf{now}}$ regions in figures 2.2 and 2.3, respectively. It is worth noting that when λ_χ the allowed region in the $x_{\mathsf{BBN}} - x_{\mathsf{now}}$ plane reduces to the dark line in figure 2.3, in which case the BBN constraint does not impose new restrictions.

It remains to see whether a gas satisfying eqn (2.27) can be in equilibrium with the SM at an epoch earlier than that of BBN. Given the small range for m_χ and the large values of x_{now} , such equilibrium could have occurred only when the gas was ultra-relativistic, in which environment the presence or absence of a condensate will have no effect. The situation then reduces to that of a standard Higgs-portal model with DM masses in the pico-eV range. Concerning direct detection experiments it is clear that for the very small masses being considered in this section the cross sections will be negligible. We will not consider these points further.

2.4   Relic abundance

In obtaining the relic abundance we will follow an approximate method that will not involve solving the Boltzmann equation. Instead we imagine the Bose gas and the SM to be in equilibrium at some early time and describe their decoupling using the Kubo formalism. As we see below, the BE gas will be non-relativistic, so that in this section the $O(\lambda_\chi)$ corrections can be ignored (see appendix).

The total Hamiltonian for the system is of the form

$$H = H_{sm} + H_{be} - H', \quad H' = -\epsilon \int d^3x \, \mathcal{O}_{sm}\mathcal{O}_{be}, \tag{2.36}$$

where $\mathcal{O}_{sm} = |\phi|^2$, $\mathcal{O}_{be} = |\chi|^2$ and ϵ is the Higgs portal coupling. We find that the temperature difference (and hence a lack of equilibrium) between the SM and Bose gas obeys

$$\dot{\vartheta} + 4\mathbb{H}\vartheta = -\Gamma\vartheta; \quad \vartheta = T_{be} - T_{sm}, \tag{2.37}$$

where $\mathbb{H}$ is the Hubble parameter. This expression is valid when $\vartheta \ll T_{be,sm}$, so the width Γ can be evaluated at the (almost) common temperature T. We use this expression to define the temperature T_d at which the SM and Bose gas decouple by the standard condition

$$T = T_d \Rightarrow \Gamma = \mathbb{H}. \tag{2.38}$$

Explicitly we have

$$\Gamma = \left(\frac{1}{c_{be}} + \frac{1}{c_{sm}}\right)\frac{\epsilon^2 G}{T}, \tag{2.39}$$

where c_{be}, c_{sm} denote the heat capacities per unit volume, T the common temperature, and

$$G = \int_0^\infty ds \int_0^\infty dt \int d^3\boldsymbol{x} \left\langle \mathcal{O}_{BE}(-is,\boldsymbol{x})\dot{\mathcal{O}}(t,\mathbf{0})\right\rangle \left\langle \mathcal{O}_{SM}(-is,\boldsymbol{x})\dot{\mathcal{O}}_{SM}(t,\mathbf{0})\right\rangle. \tag{2.40}$$

An evaluation of G is given in the Appendix. The heat capacities are given by

$$c_{sm} = \frac{4\pi^2}{30} T^3 g_{*s};$$ (2.41)

$$c = \left(\frac{m_{be}T}{2\pi}\right)^{3/2} \times \begin{cases} (15/4)\mathrm{Li}_{5/2}(1) & \text{(BEc)}, \\ (15/4)\mathrm{Li}_{5/2}(z) - (9/4)[\mathrm{Li}_{3/2}(z)]^2/\mathrm{Li}_{1/2}(z) & \text{(no BEc)}, \end{cases}$$

where Li denotes the Poly-logarithmic function, and $z = \exp[(\mu - m_\chi)/T]$.

2.5   Direct Detection

The experimentally interesting cross section of χ scattering off a nucleon can be reduced to $\eta\chi \to \eta\chi$ where η is a neutral scalar with an effective interaction

$$\mathcal{L}_{eff} = \frac{1}{2} g\eta^2 |\chi|^2$$ (2.42)

provided we make appropriate choice of g. The nucleon spin multiplicative factor will be included later.

We consider the general case where χ is a statistical ensemble, which may or may not be partially condensed. The transition probability is then

$$W_{i \to f} = |_{out}\langle f \mid i \rangle_{in}|^2$$ (2.43)

where the initial state is a spinless particle with momentum $\mathbf{p}$, and a statistical system in state $\mathcal{I}$: $|i>_{in} = a_{\mathbf{p}}^{in\,\dagger}|0; \mathcal{I}> = a_{\mathbf{p}}^{in\,\dagger}|0\rangle|\mathcal{I}\rangle$, where $|0\rangle$ denotes the vacuum for η. The final state has an η of momentum $\mathbf{q}$ and the ensemble in final state $\mathcal{F}$: $_{out}\langle f| = a_{\mathbf{q}}^{out\,\dagger}|0; \mathcal{F}\rangle =$

$a_{\mathbf{q}}^{out\,\dagger}\,|\,0\,\rangle\,|\,\mathcal{F}\,\rangle$. We require that $\mathbf{p} \neq \mathbf{q}$, since we are looking for non-trivial interactions. By the LSZ Reduction Forumla, we have

$$_{out} < f\,|i>_{in} = \langle\,0;\,\mathcal{F}\,|\,\Theta_{\mathbf{p},\mathbf{q}}\,|\,0;\,\mathcal{I}\,\rangle \qquad (2.44)$$

$$\Theta_{\mathbf{p},\mathbf{q}} = \int d^4x\,d^4x'\,e^{-ip\cdot x + iq\cdot x'}(\Box_x + m^2)(\Box_{x'} + m^2)\left(\mathcal{T}\left[\eta(x)\,\eta(x')\right]\right) \qquad (2.45)$$

where $\mathcal{T}$ is the time-ordered operator and we have neglected the renormalization factor, which will be one to lowest order.

We sum over the final states ($\mathcal{F}$), and thermally average over initial states ($\mathcal{I}$). This gives:

$$\langle W_{i \to f}\rangle = \int d^4x\,d^4x'\,d^4y\,d^4y'e^{-i(p\cdot x - q\cdot x')}e^{i(p\cdot y - q\cdot y')}(\Box_x + m^2)(\Box_{x'} + m^2)$$

$$(\Box_y + m^2)(\Box_{y'} + m^2) \qquad (2.46)$$

$$\left\langle T\left[\eta(x^0 - i\beta, \mathbf{x})\eta(x'^0 - i\beta, \mathbf{x'})\eta(y^0, \mathbf{y})\eta(y'^0, \mathbf{y'})\right]\right\rangle_\beta$$

where $\langle ...\rangle_\beta$ indicates a thermal average at temperture $1/\beta$. This can be evaluated using the real-time formalism of finite-temperature field theory [2], in particular, that complex times are later than real ones. The optical theorem relates the thermal average to the cross section as:

$$\sigma = \frac{1}{2q_{be}|\mathbf{p}|}\left(\frac{1}{\mathcal{V}}\int_{\mathbf{p}\neq\mathbf{q}}\frac{d^3\mathbf{q}}{2E_{\mathbf{q}}(2\pi)^3}\,\langle W_{i\to f}\rangle\right) \qquad (2.47)$$

where $E_{\mathbf{q}}$ is the energy of the outgoing η and $\mathcal{V}$ is the volume of space-time. To the lowest order in g, in the absence of a condensate:

$$\langle W_{i \to f} \rangle = g^2 \int \frac{d^4 k}{(2\pi)^4} \left[D^<(k+P) \right]_{ij} \left[D^>(k) \right]_{ij} \; ; \quad P = p - q. \tag{2.48}$$

The propogators have been evaluated using finite-temperature field theory and are given in eqns (A.26) and (A.29). The integration yields

$$\langle W_{i \to f} \rangle = \frac{g^2 f(-P_0)}{2\pi \beta \boldsymbol{P}} ln \left| \frac{1 + n_{be}^+(E_-)}{1 + n_{be}^+(E_+)} \frac{1 + n_{be}^-(E_-)}{1 + n_{be}^-(E_+)} \right| \tag{2.49}$$

where

$$E_\pm = \frac{1}{2} |\mathbf{P}| \sqrt{1 - \frac{4m_\chi^2}{P^2}} \mp \frac{1}{2} P_0 \tag{2.50}$$

and

$$n_{be}^\pm(E) = \left[e^{\beta(E \mp \mu)} - 1 \right]^{-1} \tag{2.51}$$

$$\langle W_{i \to f} \rangle \simeq \frac{g^2}{4\pi |\mathbf{P}| \beta} e^{-\beta E_-} \cosh(\beta \mu) . \tag{2.52}$$

The final approximation holds true in the non-relativistic regime and we have approximated $|\mathbf{p}|^2 - |\mathbf{q}|^2 \ll m_\eta$. The cross section in the non-relativistic limit is then

$$\sigma = \left[\frac{1}{\sqrt{\pi} u} e^{-u^2} + \left(1 + \frac{1}{2u^2} \right) \text{Erf}(u) \right] \sigma_0; \quad u = \frac{|\boldsymbol{p}|}{m_H} \sqrt{\frac{m_\chi}{2T}} \tag{2.53}$$

$$\sigma = \left[1 + \frac{1}{2u^2} + \mathcal{O}\left(u^{-5} e^{-u^2} \right) \right] \sigma_0, \quad (u \to \infty) \tag{2.54}$$

24

where σ_0 is the standard zero-temperature non-relativistic cross section, and we have used the fact that q_{be} is simply the number density

$$n = 2 \left(\frac{m_\chi T}{2\pi} \right)^{3/2} e^{-\beta m_\chi} \cosh\left(\beta u\right) \tag{2.55}$$

in the non-relativistic limit.

This expression is identical to the case of χ scattering off a nucleon, save for a factor of $2m_N^2$ where m_N is the mass of the nucleon. The effective coupling g includes both the Higgs portal coupling ϵ and the Higgs-nucleon coupling. In the zero-momentum-transfer limit, this is simply

$$g = \frac{\epsilon v}{m_H^2} g_{N-H} \tag{2.56}$$

where v is the SM vacuum expectation value and $g_{N-H} \simeq 0.0034$ is the Higgs-nucleon coupling [13, 27, 5].

For WIMP-range masses, that is $m_\chi \geq 1 GeV$, the present temperature of the DM gas is small, so we can make the following approximation

$$\sigma = \frac{\epsilon^2}{8\pi m_\chi^2} \left(\frac{m_\chi/m_N}{1 + m_\chi/m_N} \frac{g_{N-H} v \, m_N}{m_H^2} \right)^2 \left(1 + r^2 \frac{T_{be}}{m_\chi \mathbf{v}^2} \right); \quad r = \frac{m_H}{m_\chi} \tag{2.57}$$

$$\sigma \simeq 6.93 \times 10^{-34} \left(\frac{\epsilon}{1 + m_\chi/m_N} \right)^2 \left(1 + \frac{m_N^3}{m_\chi^3} \frac{T_{be}}{600\text{K}} \right) \text{cm}^2 \tag{2.58}$$

where $\mathbf{v} \simeq 10^{-3}$ is the relative velocity of the DM with respect to the nucleon. The temperature correction will be very small, since T_{be}, the temperature of the BE gas at the present, is very small.
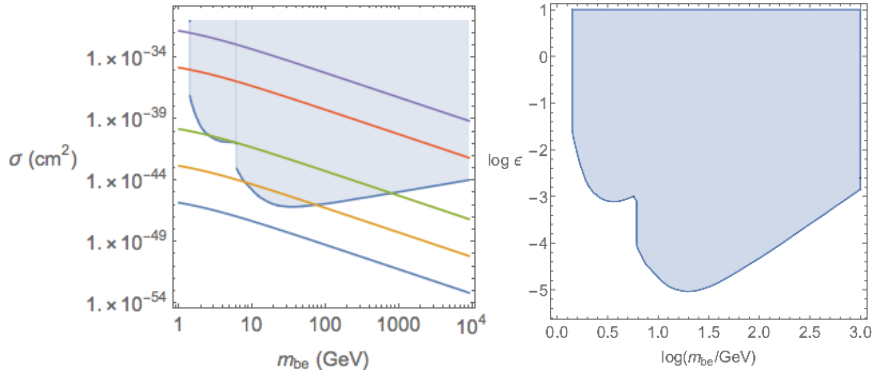
Figure 2.4: Left: the curves give the direct-detection cross section eqn (2.58) for (lower to upper curves, respectively) log ϵ = -6, -4.5, -3, -0.5, 1 with the shaded region denoting the region excluded by the XENON and CDMSLite experiments. Right: the shaded area denotes the region of the $m_\chi - \epsilon$ plane excluded by the direct-detection.

A comparison of our parameter space to the experimental constraints from XENON [7] and CDMSLite [6], which give the strongest constraints on this model, can be seen in fig. 2.4. That is to say, we can fix μ to satisfy relic abundance constraints (not discussed here), provided that the parameters are permitted by direct-detection constraints.

So far we have assumed that no condensate is present. In the case where a nucleon scatters off a system made up of both BEc and gas, the result must be solved numerically, but can be shown to give the above expression in the limit where the condensate goes to zero. However, without external considerations (ie, potential gravitational effects within galaxies), we find that m_χ must be well below the WIMP mass range in order to maintain a condensate in the present epoch. Nevertheless, for completeness, we include the calculation of the cross section in the case when a condensate exists.

In this case, we write the complex field χ in the presence of a condensate as $\chi \to [(A_1 + C) + iA_2]/\sqrt{2}$ and follow a similar process to that above. To lowest order, we obtain

$$\langle W_{i\to f}\rangle_\beta = C^2 \int d^4x \, d^4y \, e^{-i(p-q)\cdot(x-y)} \, \langle T_C \left[A_1 \left(t - i\beta, \boldsymbol{x} \right) A_1(y) \right] \rangle_\beta$$

$$+ \frac{1}{4} \int d^4x \, d^4y \, e^{-i(p-q)\cdot(x-y)} \{ \langle T_C \left[\boldsymbol{A}^2 \left(t - i\beta, \boldsymbol{x} \right) \boldsymbol{A}^2(y) \right] \rangle_\beta \qquad (2.59)$$

$$- \langle \boldsymbol{A}^2 \rangle_\beta^2 \},$$

where, as before, we have assumed that $p \neq q$. Using eqns (A.26) and (A.29), we find

$$\frac{1}{\mathcal{V}} \langle W_{i\to f}\rangle = C^2 D_{11}^{>}(P)|_{\mu=m_\chi} + \frac{g^2 T f(-P_0)}{2\pi |\boldsymbol{P}|} \ln \left| \frac{1 + n_{be}^{+}(E_-)}{1 + n_{be}^{+}(E_+)} \frac{1 + n_{be}^{-}(E_-)}{1 + n_{be}^{-}(E_+)} \right|_{\mu=m_\chi}, \qquad (2.60)$$

where $n_{be}^{\pm}$ are defined in eq (2.51) and $E_\pm$ in eqn (2.50). Then the total cross section is given by

$$\sigma = \sigma^{(1)} + \sigma^{(2)} \qquad (2.61)$$

$$\sigma^{(1)} = \frac{q_{be}^{(c)}}{2m_\chi |\boldsymbol{p}| q_{be}} \int' \frac{d^3\boldsymbol{q}}{2E_{\boldsymbol{q}}(2\pi)^3} D_{11}^{>}(P)|_{\mu=m_\chi}; \quad E_{\boldsymbol{q}} = \sqrt{\boldsymbol{q}^2 + m_\eta^2}, \qquad (2.62)$$

$$\sigma^{(2)} = \frac{1}{2q_{be}|\boldsymbol{p}|} \int' \frac{d^3\boldsymbol{q}}{2E_{\boldsymbol{q}}(2\pi)^3} \frac{g^2 T f(-P_0)}{2\pi |\boldsymbol{P}|} \ln \left| \frac{1 + n_{be}^{+}(E_-)}{1 + n_{be}^{+}(E_+)} \frac{1 + n_{be}^{-}(E_-)}{1 + n_{be}^{-}(E_+)} \right|_{\mu=m_\chi}, \qquad (2.63)$$

where $E_{\boldsymbol{q}}$ is the energy of the outgoing η, q_{be} is merely the number density of the Bose gas particles since we are working in the non-relaticistic limit, and we used $q_{be}^{(c)} = m_\chi C^2$ as the number density in the condensate. The prime on the integral indicates that we exclude the forward scattering $p = q$ region.

27

For $m_\eta \neq m_\chi$ in the non-relativistic limit,

$$\sigma^{(1)} = -\frac{Tn_0/n}{32\pi m_\chi \boldsymbol{p}^2} ln\left|f\left(-\mathcal{E}_-\right)f\left(\mathcal{E}_+\right)\right|; \quad \mathcal{E}_\pm = \frac{2m_\chi \boldsymbol{p}^2}{m_\chi^2 + m_\eta^2 \pm 2m_\chi \bar{E}_{\boldsymbol{p}}}, \qquad (2.64)$$

where $\bar{E}_{\boldsymbol{p}} = \sqrt{m_{be}^2 + \mathbf{p}^2}$ and f is given in eqn (A.29). In general $\sigma^{(1)}$ is not positive definite, but in the case where $T \to 0$, it reduces to the standard result $\sigma^{(1)} \to [16\pi(m_\chi + m_\eta)^2]^{-1}$ and is greater than 0 for all parameters of interest.

Evaluating the expression for $\sigma^{(2)}$ is more complex. Using the non-relativistic expression for $E_\pm$

$$E_\pm = m_\chi + \frac{1}{8m_\chi |\boldsymbol{P}|^2}\left[|\boldsymbol{P}|^2 \mp \frac{m_\chi}{m_\eta}(\boldsymbol{p}^2 - \boldsymbol{q}^2)\right]^2 \qquad (2.65)$$

and defining new integration variables

$$w = \frac{|\boldsymbol{P}|}{|\boldsymbol{p}|}, \quad z = \frac{1}{w}\left(\frac{|\boldsymbol{q}|^2}{|\boldsymbol{p}|^2} - 1\right)\frac{m_\eta}{m_\beta}, \qquad (2.66)$$

we find

$$\sigma^{(2)} = \frac{T|\boldsymbol{p}|}{256\pi^3 q_{be} m_\chi} \int_0^\infty dw\, w \int_{(w-2)m_\chi/m_\eta}^{(w+2)m_\chi/m_\eta} \frac{dz}{exp\left\{4lwz\right\} - 1}$$
$$\times ln\left|\frac{1 - exp\left\{-l\left(w + z\right)^2\right\}}{1 - exp\left\{-l(w - z)^2\right\}}\right|, \qquad (2.67)$$

where $l = \beta|\boldsymbol{p}|^2/(8m_\chi)$. In general, this is not analytically solveable; for moderate values of l it must be solved numerically, but for $l \to \infty$ it reduces to eqn (2.58).

Chapter 3

Neutrino Portal Self-Interacting Dark Matter

3.1 The Model

We apply a slight variation to the neutrino portal dark matter model [10] to include self-interaction. The original model contains one heavy dark scalar Φ and one fermion Ψ. Since we take $m_\Phi > m_\Psi$, the Φ will all decay to Ψ, leaving only Ψ in the present epoch as the dark matter candidate. The dark sector interacts with the Standard Model via a new mediator fermion $\mathcal{F}$, which mixes with the SM neutrino. Provided that we require $m_\Psi \lesssim 35\text{GeV}$ and $\mathcal{F} \gtrsim \mathcal{O}(200\text{GeV})$, the model is consistent with current experimental limits.

We extend the model by adding a $U(1)_{dark}$ gauge symmetry with vector boson, V, which couples to Ψ. To prevent the V from mixing with the SM photon, we also include a dark $\mathbb{Z}_2$ symmetry under which V is odd and all SM particles are even. Furthermore,

we introduce one new fermion and replace $\Psi \to \Psi_1$, Ψ_2. Under the $\mathbb{Z}_2$ symmetry, the lagrangian is invariant for:

$$\Psi_1 \to \Psi_2$$

$$\Phi \to \Phi*$$

$$V \to -V$$

The symmetry therefore requires that Ψ_1 and Ψ_2 have the same mass and couplings and implies that V is stable. The latter produces conflicts with experimental constrains, which we address below. We therefore require that the $\mathbb{Z}_2$ symmetry be softly broken. To do this, we introduce a mass splitting, μ, between $\Psi_{1,2}$.

$$\begin{aligned}
\mathcal{L} = &\bar{\Psi}_1(i\slashed{D}_1 - m_1)\Psi_1 + \bar{\Psi}_2(i\slashed{D}_2 - m_2)\Psi_2 + |D\Phi|^2 - \frac{1}{2}m_\Phi|\Phi|^2 - \frac{1}{4}\lambda|\Phi|^4 \\
&- \frac{1}{4}V_{\mu\nu}V^{\mu\nu} + \frac{1}{2}m_v^2(V_\mu - \frac{1}{m_V}\partial_\mu\sigma)^2 + \bar{\mathcal{F}}(i\slashed{\partial} - m_\mathcal{F})\mathcal{F} - (\bar{l}Y^{(\nu)}\mathcal{F}\tilde{\phi} + h.c.) \quad (3.1) \\
&- z((\bar{\Psi}_1\Phi\mathcal{F} + \bar{\Psi}_2\Phi^*\mathcal{F}) + h.c.) - \lambda_x|\Phi|^2|\phi|^2
\end{aligned}$$

Where $D_{1,2} = \partial \pm igV$ is the covariant derivative, $m_{1,2} = m_\Psi \pm \mu$, and ϕ is the SM scalar isodoublet. We have given V mass via the Stuckelberg mechanism with σ as the Stuckelberg field, and we assume that $m_V > m_\Psi$, which we will justify later. $\mathcal{F}$ carries a family index, indicating 3 fields, and therefore $m_\mathcal{F}$ and $Y^{(\nu)}$ are both 3×3 matrices while z is a 3×1 coupling vector. For simplification, we assume that all z are real.

After spontaneous symmetry breaking in the standard model, the lagrangian will contain mixing terms between the left-handed neutrino and $\mathcal{F}$. We label the mass eigenstates as n_L and N for the massless, left-handed fermions and the fermions of mass $\mathcal{O}(m_\mathcal{F})$,

respectively, and identify n_L with the standard model neutrinos. To simplify the model, we assume that N are degenerate with mass m_N. The relationship between gauge fields and mass eigenstates is given by:

$$\mathcal{F} = \mathcal{C}N_L + \mathcal{S}n_L + N_R \tag{3.2}$$

$$\nu = V_{PMNS}^{\dagger}(\mathcal{C}n_L - \mathcal{S}N_L) \tag{3.3}$$

where V_{PMNS} is the PMNS matrix and $\mathcal{C}$ and $\mathcal{S}$ are diagonal 3×3 matrices, which satisfy

$$\mathcal{C}^2 + \mathcal{S}^2 = \mathbf{1}. \tag{3.4}$$

3.2 DM self-interactions:

We consider all possibilities for interaction between two Ψ_i particles (note that we exclude $\bar{\Psi}\Psi$ interactions, since in the the modern universe we expect most $\bar{\Psi}$ particles to have annihilated away, thus leaving these interactions insignificant, and we furthermore neglect μ and assume Ψ_1 and Ψ_2 are degenerate). In other words, we consider $\Psi_i\Psi_j \to \Psi_i\Psi_j$ for both $i = j$ and $i \neq j$. The first is the same case as Moller scattering with a massive photon (fig 3.1); since the photon is massive, we can integrate this to find the total velocity-dependent cross section in the nonrelativistic limit:

$$\sigma_{eq}(v) = \frac{g^4}{16m^2 m_V^2 \pi v^2 (2 + v^2)^2 a \left(m_V^2 + b\right) \left(2m_V^2 + b\right)}$$

$$\{2b \left(2m_V^2 + b\right) \left[2m_V^4 + 2m_\Psi^4 (2 + 4v^2 + v^4)^2 + c\right] \tag{3.5}$$

$$+ 4m_V^2 \left(m_V^2 + b\right) \left[2m_V^4 + 4m_\Psi^4 (1 + 4v^2 + v^4) + c\right] ln \left[\frac{m_V^2}{m_V^2 + b}\right]\}$$

$$a = (4 + v^2); \quad b = m_\Psi^2 v^2 a; \quad c = m_V^2 \left(8m_\Psi^2 + 3b\right) \tag{3.6}$$

Similarly, we can find the interaction cross section for Ψ_1 scattering off of Ψ_2:

$$\sigma_{neq}(v) = \frac{g^4}{32m_\Psi^2 \pi b (2 + v^2)^2} \{\frac{4b(2m_V^4 + 2m_\Psi^4 (2 + 4v^2 + v^4)^2 + c)}{m_V^2 (m_V^2 + b)}$$

$$+ 8(m_V^2 + m_\Psi^2 (2 + v^2)^2)ln \left[\frac{m_V^2}{m_V^2 + b}\right]\} \tag{3.7}$$

where the subscript eq or neq indicates $i = j$ or $i \neq j$, respectively. When $m_\Psi \gg m_V$ and the relative velocity is small, these interactions will satisfy the SIDM requirements to reproduce core-shaped density distributions within galaxies. Since $\Psi_{1,2}$ have approximately equivalent masses and identical couplings, each will have the same abundance, making up half of the observed relic abundance. Furthermore, the total $\Psi_i \Psi_j \rightarrow \Psi_i \Psi_j$ cross section will simply be the average of σ_{eq} and σ_{neq}.

Experimental limits are placed on the self-interaction cross section from core v. cusp data in galaxies and clusters. These two average values of $\sigma(v)$ (for galaxies and clusters, respectively) allow us to solve for $m_V(m_\Psi)$ and $g(m_\Psi)$:

$$m_V = \frac{m_\Psi}{443}; \quad g = \left(\frac{m_\Psi}{63}\right)^{3/4} \tag{3.8}$$

32
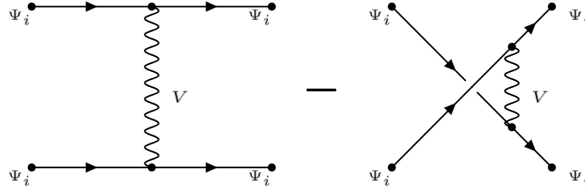
Figure 3.1:

We do not include the dark photon in the self-interaction limit, though it is massive, for reasons discussed below. These expressions for m_V and g have significant errors, which we esitmate using [29]:

$$443 \to (116,\ 1557) \quad 64\text{GeV} \to (17,\ 225)\text{GeV}. \tag{3.9}$$

For numerical purposes, we assume the values in eqn (3.8) are uncertain up to a factor of 3.

3.3   Decay of the V

In the absence of the $\mathbb{Z}_2$ symmetry breaking, the massive dark photon presents something of a problem. Once it decouples from the Ψ, its abundance is fixed since the V would have no mechanism by which to decay. Furthermore, it has no tree-level self-interactions, which adds complications both to abundance and core v cusp restrictions. Furthermore, given that the V is light, we encounter conflicts with both Big Bang Nucleosynthesis (BBN) constraints and large scale structure formation [16, 19].

One possible solution is the ensure that V can decay into SM particles with some small cross section. There is such a decay in our model (fig. 3.2) at one loop, but vanishes
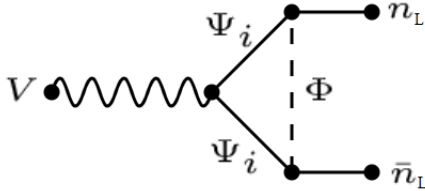
Figure 3.2: Graphs responsible for a non-zero decay width for the V.

if the Ψs are degenerate. To rememdy this, we choose to softly break our $\mathbb{Z}_2$ symmetry by adding to the lagrangian a term of the form:

$$-\mu\bar{\Psi}_1\Psi_1 + \mu\bar{\Psi}_2\Psi_2 \tag{3.10}$$

Then we calculate the decay width, assuming $m_\Psi \gg m_V$, when all external momenta are zero.

$$\Gamma(V \to \bar{n}_L n_L) = \frac{m_V}{6\pi}\left\{\frac{g}{16\pi^2}\left[f\left(\frac{m_1}{m_\Phi}\right) - f\left(\frac{m_2}{m_\Phi}\right)\right]\right\}^2 \left(z\boldsymbol{S}^2 z^\dagger\right)^2 \tag{3.11}$$

$$f(x) = \frac{1}{4}\left(\frac{x^2+1}{x^2-1}\right) - \left(\frac{x^2}{x^2-1}\right)^2 \ln x \tag{3.12}$$

Experimental limits on this decay width are very soft; provided that the lifetime of $V \lesssim 1s$, the Vs will decay rapidly enough to not contribute to the relic density or interfere with BBN or structure formation. This corresponds to a mass difference $m_1 - m_2 \gtrsim 0.1 MeV$.

34

3.4 Bound States

The inclusion of an interaction between oppositely-charged $\Psi_{1,2}$ particles opens up the possibility that $\Psi_{1,2}$ will form bound states. In the regime where this occurs, the core v cusp problem reappears; since the self-interaction would be screened, we expect the cusp-shaped density profile to reappear. In order to circumvent this problem, we consider the region of parameter space where a bound state does not form.

In the nonrelativistic case, $\Psi_{1,2}$ experience a Yukawa interaction of the form

$$\mathcal{V}_{NR} = \frac{g^2}{4\pi} \frac{3^{-m_V r}}{r}, \tag{3.13}$$

which will provide potential energy $\sim \frac{g^2 m_V}{4\pi}$. To prevent a bound state from forming, the potential energy must be smaller than the kinetic energy ($\sim \frac{m_V^2}{m_\Psi}$). Therefore, we require $\frac{g^2 m_V}{4\pi} < \frac{m_V^2}{m_\Psi}$. Utilizing the limits on m_V and g acquired above, we find

$$0.595 \frac{g^2}{4\pi} < \frac{m_V}{m_\Psi} \tag{3.14}$$

$$\Rightarrow m_\Psi < 8.4 \text{GeV} \tag{3.15}$$

which is uncertain up to a factor of ~ 6. For the numeric calculations below, we use $m_\Psi < 10$GeV. That is, in order to circumvent the issue of bound states causing screened self-interaction among DM particles, $\Psi_{1,2}$ must have mass less than $\mathcal{O}(10 GeV)$. It is intersting to note that this preferred region of parameter space may well be hidden below the neutrino floor, which rises up below $\sim \mathcal{O}(10 \text{GeV})$.

3.5   Electroweak Constraints

Due to the mixing of the Standard Model neutrino with the fermionic mediators, $\mathcal{F}$, the invisible decay of the Z and the Higgs, and W-mediated decays provide constraints on our model parameters. Below, we discuss constraints from these three processes individually.

3.5.1   Z invisible Decay

The addition of singlet Dirac fermions N to the SM generates non-universal, though flavor diagonal, neutrino (n) couplings to the Z proportional to $\mathcal{C}^2$. The invisible $Z \to nn$ width will be proportional to $\text{tr}(\mathcal{C}^2)$; since experimental results indicate [3] $\Gamma(Z \to inv) = 499.0 \pm 1.5 MeV$, we will have stringent bounds on our parameters. The effective coupling between Ψ_i and Z in our model will be of the form $\bar{\psi}_1 \not{Z}(a + b\gamma_5)\psi_2$, where ψ is a fermion, so we find

$$
\begin{aligned}
\Gamma(Z \to \psi_1 \psi_2) = {} & \frac{(|a|^2 + |b|^2)m_Z}{24\pi} \\
& \times \left[2 - r_{1z} - r_{2z} - (r_{1z} - r_{2z})^2 - 6\frac{|a|^2 - |b|^2}{|a|^2 + |b|^2}\sqrt{r_{1z}r_{2z}} \right] \sqrt{\lambda(1,\ r_{1z},\ r_{2z})}
\end{aligned}
\tag{3.16}
$$

where $\lambda(u,\ v\ w) = u^2 + v^2 + w^2 - 2uv - 2vw - 2wu$ and r_{ab} is the squared mass ratio of particles a and b, $r_{ab} = m_a^2/m_b^2$. We take N to be degenerate and obtain

$$
\Gamma(Z \to nn) = \Gamma_0 \text{tr}\{\mathcal{C}^4\}, \quad \Gamma_0 = \left(\frac{g}{2\cos\theta_W}\right)^2 \frac{m_Z}{24\pi}
\tag{3.17}
$$

$$
\Gamma(Z \to NN) = \Gamma_0 tr\{\mathcal{S}^4\}(1 - r_{NZ})\sqrt{1 - 4r_{NZ}}\,\theta(1 - 4r_{NZ})
\tag{3.18}
$$

$$\Gamma(Z \to Nn) = \Gamma_0 tr\{\mathcal{C}^2 \mathcal{S}^2\}(2 + r_{NZ})(1 - r_{NZ})^2 \theta(1 - r_{NZ}) \tag{3.19}$$

Current experimental limits require that

$$\left| \frac{\Gamma(Z \to inv)}{\Gamma_{SM}(Z \to inv)} - 1 \right| < 0.0093. \tag{3.20}$$

In terms of our parameters, this indicates

$$\frac{1}{3}[-tr\left\{\mathcal{S}^2\left(\mathbf{1} + \mathcal{C}^2\right)\right\} + tr\left\{\mathcal{S}^4\right\}(1 - r_{NZ})\sqrt{1 - 4r_{NZ}}\theta(1 - 4r_{NZ})$$
$$+ tr\left\{\mathcal{C}^2 \mathcal{S}^2\right\}(2 + r_{NZ})(1 - r_{NZ})^2 \theta(1 - r_{NZ})] < 0.0093. \tag{3.21}$$

3.5.2 H invisible decays

A general coupling of the form $\bar{\psi}_1(a + b\gamma_5)\psi_2 H + h.c.$ gives

$$\Gamma(H \to \psi_1 \psi_2) = \frac{\sqrt{\lambda(m_H^2, m_1^2, m_2^2)}}{8\pi m_H^3} \left[\left(|a|^2 + |b|^2\right)\left(m_H^2 - m_1^2 - m_2^2\right) - 2\left(|a|^2 - |b|^2\right)m_1 m_2 \right] \tag{3.22}$$

from which we can obtain:

$$\Gamma(H \to \bar{\Psi}\Psi) = \frac{m_H \epsilon_H^2}{8\pi}(1 - 4r_{\Psi H})^{3/2}\theta(1 - r_{\Psi H}), \tag{3.23}$$

$$\Gamma(H \to nN) = \frac{m_H^3}{4\pi v_H^2}[r_{NH}(1 - r_{NH})tr\left\{\mathcal{S}^2 \mathcal{C}^2\right\}\theta(1 - r_{NH})$$
$$+ \frac{1}{2}(1 - 4r_{NH})^{3/2}tr\left\{\mathcal{S}^4\right\}\theta(1 - 4r_{NH})], \tag{3.24}$$

$$\Gamma(H \to \Phi\Phi) = \frac{(v_H^2 \lambda_x)}{16\pi m_H} \sqrt{1 - 4r_{\Phi H}} \theta(1 - 4r_{\Phi H}), \tag{3.25}$$

the first of which is negligible due to the ϵ_H^2 prefactor.

From experimental constraints, we can then write

$$
4.89 \times 10^{-4} > |r_{NH}(1 - r_{NH})tr\left\{\mathcal{S}^2\mathcal{C}^2\right\}\theta(1 - r_{NH}) + \frac{1}{2}(1 \\
- 4r_{NH})^{3/2}tr\left\{\mathcal{S}^2\right\}\theta(1 - 4r_{NH}) + 1.93\lambda_x^2\sqrt{1 - 4r_{\Phi H}}\theta(1 - r_{\Phi H})|. \tag{3.26}
$$

3.5.3 W-mediated decays

Due to mixing with the SM neutrino, W boson interactions with charged leptons are also changed. The vertex involving a charged lepton e_{Lr} and a neutrino mass eigenstate n_{Ls}, where we have used r and s as flavor indices, gains a factor of $\left(V_{PMNS}^\dagger \mathcal{C}\right)_{rs}$. Assuming $m_N > m_\tau$,

$$\Gamma(l_r \to l_s \bar{\nu}\nu) \simeq (1 - \Delta_r - \Delta_s)\Gamma_{SM}(l_r \to l_s \bar{\nu}\nu); \quad \Delta_r = \left(V_{PMNS}^\dagger \mathcal{S}^2 V_{PMNS}\right)_{rr} > 0. \tag{3.27}$$

We define $R_{u \to X} = B(u \to X)/B_{SM}(u \to X) - 1$. For the decays of interest:

$$R_{\tau \to \mu\nu\bar{\nu}} \simeq B_{SM}(\tau \to e\nu\bar{\nu})\Delta_e - [1 - B_{SM}(\tau \to \mu\nu\bar{\nu})]\Delta_\mu \Rightarrow |0.8223\Delta_\mu - 0.1958\Delta_e| \leq 0.0069$$

$$\tag{3.28}$$

$$R_{e\nu\bar{\nu}} \simeq B_{SM}(\tau \to \mu\nu\bar{\nu})\Delta_\mu - [1 - B_{SM}(\tau \to e\nu\bar{\nu})]\Delta_e \Rightarrow |0.1777\Delta_\mu - 0.8042\Delta_e| \leq 0.0067$$

$$\tag{3.29}$$

$$R_{\pi \to \mu\nu} \simeq B_{SM}(\pi \to e\nu)(\Delta_\mu - \Delta_e) \Rightarrow |\Delta_\mu - \Delta_e| \leq 0.010 \qquad (3.30)$$

to 3σ.

3.6   Muon anomalous magnetic moment

The new NNW vertices, and the $\mathcal{C}$ factors for the nnW vertices generate contribution to the anomalous magnetic moment of the muon, a_μ. Using the results of [18] it is straightforward to see that

$$\Delta a_\mu = \frac{G_{\mathrm{F}}\, m_\mu^2}{\sqrt{2}\, 8\pi^2} \Delta_\mu \left[F(r_{\mathrm{NW}}) - F(0) \right] , \qquad (3.31)$$

where $\Delta_\mu = \Delta_{r=2}$ is defined in eqn (3.27) and

$$F(w) = \int_0^1 dx \frac{2x^2(1+x) + x(1-x)(2-x)w - x^2(x-1)k}{kx^2 + (1-k)x + (1-x)w} ; \quad k = \left(\frac{m_\mu}{m_W} \right)^2 , \qquad (3.32)$$

$$\simeq \int_0^1 dx \frac{2x^2(1+x) + x(1-x)(2-x)w}{x + (1-x)w} \qquad (3.33)$$

so that

$$F(w) - F(0) \simeq \frac{10 - 33w + 45w^2 - 4w^3}{6(1-w)^3} + \frac{3w^3 \ln w}{(1-w)^4} - \frac{5}{3}, \qquad (3.34)$$

and this ranges from 0 when $w = 0$ to -1 when $w \to \infty$. Then

$$|\Delta a_\mu| \leq \frac{G_{\mathrm{F}}\, m_\mu^2}{\sqrt{2}\, 8\pi^2} \Delta_\mu = 1.17 \times 10^{-9} \Delta_\mu . \qquad (3.35)$$

The constraints derived form W-mediated decays require $\Delta_\mu \lesssim 10^{-2}$ so $|\Delta a_\mu| \lesssim 10^{-11}$, while the current error is $(\pm 5.4 \pm 3.3) \times 10^{-10}$. The anomalous magnetic moment limits do not produce a competitive bound now, but may do so with the upgraded Fermilab experiment.

3.7 Direct Detection

We calculate the scattering cross section for a Ψ_i scattering off a nucleon. The cross section receives contribution from both the Higgs and the Z Boson. The relevant effective operators are (in the small momentum transfer limit):

$$\mathcal{L}_{DM-n,p}^{(Z)} = \sqrt{2} G_F \left[\bar\Psi \gamma_\mu (\epsilon_L P_L + \epsilon_R P_R) \Psi \right] \left[\bar{\boldsymbol{p}} J_p^\mu \boldsymbol{p} + \bar{\boldsymbol{n}} J_n^\mu \boldsymbol{n} \right] + O(q^2) \qquad (3.36)$$

$$\mathcal{L}_{DM-n,p}^{(H)} = G_H \left[\bar{\boldsymbol{p}}\boldsymbol{p} + \bar{\boldsymbol{n}}\boldsymbol{n} \right] \bar\Psi \Psi + O(q^2); \quad G_H = -\frac{0.011 \epsilon_H}{m_H^2} \qquad (3.37)$$

The nucleon currents, $J_{n,p}^\mu$, are given by

$$\mathcal{J}_p^\mu = \frac{1}{2} \left[\left(1 - 4\sin^2\theta_w \right) \gamma^\mu + g_A \left(\gamma^\mu - \frac{2m_\mathcal{N} q^\mu}{m_{pi}^2 + \boldsymbol{q}^2} \right) \gamma_5 \right] \qquad (3.38)$$

$$\mathcal{J}_n^\mu = -\frac{1}{2} \left[\gamma^\mu + g_A \left(\gamma^\mu - \frac{2m_\mathcal{N} q^\mu}{m_{pi}^2 + \boldsymbol{q}^2} \right) \gamma_5 \right] \qquad (3.39)$$

where $m_\mathcal{N}$ is the nucleon mass and $\boldsymbol{q}$ is the momentum transfer.

In the non-relativistic limit, the effective lagrangian becomes

$$\mathcal{L}_{nucleon-DM}|_{NR} = 4G_H \mathbf{1}_\Psi \mathbf{1}_\mathcal{N}$$

$$+ \sqrt{2} G_F \left(\epsilon_R + \epsilon_L \right) \left\{ \left[-2\sin^2\theta_w + \left(1 - 2\sin^2\theta_w \right) \tau_3 \right] \mathbf{1}_\Psi \mathbf{1}_\mathcal{N} \right. \tag{3.40}$$

$$\left. + \tau_3 \left[\boldsymbol{s}_\Psi \cdot \boldsymbol{s}_\mathcal{N} - 4\frac{\left(\boldsymbol{q} \cdot \boldsymbol{s}_\Psi \right) \left(\boldsymbol{q} \cdot \boldsymbol{s}_\mathcal{N} \right)}{m_\pi^2 + \boldsymbol{q}^2} \right] \left(\frac{\epsilon_R - \epsilon_L}{\epsilon_R + \epsilon_L} \right) g_A \right\}$$

where τ_3 is 1 for protons and -1 for neutrons, $\boldsymbol{s}_{\Psi,\mathcal{N}}$ are the spin operators for the DM and nucleons, respectively. The DM-nucleus cross section is then calculated using the procedure detailed in [8], and is found to be:

$$\sigma_\mathbb{N} = \frac{(m_\mathbb{N}/m_\mathcal{N})^2}{16\pi(m_\mathbb{N} + m_\Psi)^2}$$

$$\left\{ \kappa^2 \left[(1+b)^2 F_M^{(p,p)} + (1-b)^2 F_M^{(n,n)} + 2 (1-b)^2 F_M^{(p,n)} \right] \right.$$

$$+ \frac{\mathbb{K}^2 \left(Q^2 - 2Q + 3 \right)}{12} \tag{3.41}$$

$$\left. \left[F_{\Sigma''}^{(p,p)} + F_{\Sigma''}^{(n,n)} - 2F_{\Sigma''}^{(p,n)} + 2 \left(F_{\Sigma'}^{(p,p)} + F_{\Sigma'}^{(n,n)} - 2F_{\Sigma'}^{(p,n)} \right) \right] \right\}$$

we use $m_\mathbb{N}$ to denote the nuclear mass and

$$\kappa = \sqrt{2} G_F m_\Psi m_\mathcal{N} \left[2 \left(\epsilon_L + \epsilon_R \right) \sin^2\theta_w - 2\sqrt{2}\frac{G_H}{G_F} \right], \quad Q = \frac{4|\boldsymbol{q}|^2}{|\boldsymbol{q}|^2 + m_\pi^2}, \tag{3.42}$$

$$\mathbb{K} = \frac{G_f \left(\epsilon_R - \epsilon_L \right) m_\Psi m_\mathcal{N}}{\sqrt{2}} g_A, \quad b = \frac{1 - 2\sin^2\theta_w}{\sqrt{8}G_H / \left[\left(\epsilon_L + \epsilon_R \right) G_F \right] - 2\sin^2\theta_w} \tag{3.43}$$

From this, we can acquire the DM-nucleon cross section:

$$\sigma_\mathcal{N} = \left(\frac{m_\mathcal{N}}{m_\mathbb{N}} \right)^2 \left(\frac{m_\Psi + m_\mathbb{N}}{m_\Psi + m_\mathcal{N}} \right)^2 \frac{1}{\mathcal{A}^2} \sigma_\mathbb{N} \tag{3.44}$$

where $\mathcal{A}$ is the atomic number.

For systems made up of multiple isotopes, I, with abundances α_I, $F_X^{(N,N')} \rightarrow^I$ $F_X^{(N,N')}$ and

$$\frac{1}{\mathcal{A}^2} F_X^{(N,N')} \rightarrow \sum_I \frac{\alpha_I}{\mathcal{A}_I^2}{}^I F_X^{(N,N')} = f_X^{(N,N')} \tag{3.45}$$

so that, with the following definitions

$$f_1 = f_M^{(p,p)} + f_M^{(n,n)} + 2 f_M^{(p,n)} \tag{3.46}$$

$$f_2 = f_M^{(p,p)} - f_M^{(n,n)} \tag{3.47}$$

$$f_3 = f_M^{(p,p)} + f_M^{(n,n)} - 2 f_M^{(p,n)} \tag{3.48}$$

$$f_4 = \left(f_{\Sigma''}^{(p,p)} + f_{\Sigma''}^{(n,n)} - 2 f_{\Sigma''}^{(p,n)} \right) + \left(f_{\Sigma'}^{(p,p)} + f_{\Sigma'}^{(n,n)} - 2 f_{\Sigma'}^{(p,n)} \right) \tag{3.49}$$

we can write the DM-nucleon cross section as

$$\sigma_{\mathcal{N}} = \frac{1}{16\pi^2 (m_{\mathcal{N}} + m_{\Psi})^2} \left[\left(f_1 + 2b f_2 + b^2 f_3 \right) \kappa^2 + \frac{\mathbb{K}^2 \left(Q^2 - 2Q + 3 \right)}{12} f_4 \right]. \tag{3.50}$$

The suppression of the spin-dependent contribution, which is given by the term proportional to $\mathbb{K}^2$, with respect to the spin-independent contribution, which is given by the term proportional to κ^2, is due to the fact that $f_1 \gg f_4$.

3.8 Relic Abundance

The two dark matter candidates, Ψ_1 and Ψ_2 have approximately equal mass and couplings with the V. Their interactions will allow them to remain in equilibrium with each other even after the dark sector has decoupled from the SM. As such, we take their respective abundances to be the same and perform the relevant calculation for one Ψ_i abundance only. We label $\rho_\Psi = \frac{1}{2}\rho_1 = \frac{1}{2}\rho_2$. The interactions of interest are $\bar{\Psi}_1 \Psi_1 \to \bar{n}_L n_L$ and $\Psi_1 \Psi_2 \to n_L n_L$, both of which have the same cross section, and $\bar{\Psi}\Psi \to VV$. With this in mind, we use only one neutrino cross section in the calculation below and include a factor of 2 in the final result.

We follow the usual perscription for calculating abundance with the Boltzmann Equation:

$$\frac{dn_\Psi}{dt} + 3H n_\Psi = \sigma_0 \left[n_\Psi^2 - \left(n_\Psi^{(eq)} \right)^2 \right] \tag{3.51}$$

where n_Ψ refers to the number density for Ψ and

$$\sigma_0 = \frac{1}{2} \langle \sigma v \rangle_{\bar{\Psi}\Psi \to nn} + \frac{1}{4} \langle \sigma v \rangle_{\bar{\Psi}\Psi \to VV} \tag{3.52}$$

The relevant cross sections contain only diagram each (t-channel Φ exchange and t-channel Ψ exchange, respectively), illustrated in fig. 3.3, which we calculate to be:

$$\sigma_{\bar{\Psi}_1 \Psi_1 \to \bar{n}_L n_L} = \frac{(z\mathcal{S}^2 z^{\mathrm{T}})^2}{64\pi s \beta_\pi} \left[\frac{1 + 2y(1+y) - \beta_\Psi^2}{(1+y)^2 - \beta_\Psi^2} + \frac{y}{\beta_\Psi} \ln \left(\frac{1 - \beta_\Psi + y}{1 + \beta_\Psi - y} \right) \right] \tag{3.53}$$

43

$$\sigma_{\bar{\Psi}\Psi \to VV} = \frac{g^4}{8\pi s} \frac{\beta_V}{\beta_\Psi} \left[\frac{sm_\Psi^2 + 4\left(m_V^4 - 2m_V^2 m_\Psi^2 - 2m_\Psi^4\right)}{sm_\Psi^2 + m_V\left(m_V^2 - 4m_\Psi^2\right)} \right.$$
$$\left. + \frac{4\left(m_V^2 + m_\Psi^2\right)}{s\beta_V\beta_\Psi} ln\left|\frac{1 + \beta_V^2 + 2\beta_\Psi\beta_V}{1 + \beta_V^2 - 2\beta_\Psi\beta_V}\right| \right] \tag{3.54}$$

where

$$y = \frac{2(m_\Phi^2 - m_\Psi^2)}{s}; \quad \beta_i = \sqrt{1 - \frac{4m_i^2}{s}}. \tag{3.55}$$

Given that other constraints require our DM mass be small, that is $m_\Psi < m_H$, m_Z, we will have no resonant contributions to this cross section and can use the usual approximations [17]. Thus we find

$$\langle \sigma v \rangle_{\bar{\Psi}_1\Psi_1 \to nn} \simeq \frac{\left(z\mathcal{S}^2 z^{\mathrm{T}}\right)^2}{32\pi(r_{\Phi\Psi} + 1)^2 m_\Psi^2} = \sigma_0 \tag{3.56}$$

$$\langle \sigma v \rangle_{\bar{\Psi}\Psi \to VV} \simeq \frac{g^4}{16\pi m_\Psi^2} \tag{3.57}$$

where all neutrino final states have been summed over and we take $m_\Psi \gg m_V$. Then we find the combined cross section (eqn (3.52)) to be:

$$\sigma_0 = \frac{g^4 + \left[z\mathcal{S}z^{\mathrm{T}}/(r_{\Psi\Phi} + 1)\right]^2}{64\pi m_\Psi^2} \tag{3.58}$$

Using the standard freeze-out approximation [17], the relic abundance is given by:

$$\Omega_\Psi h^2 = \frac{1.07 \times 10^9}{\mathrm{GeV}} \frac{x_f}{g_{*s}\xi}; \quad \xi = \frac{M_{Pl}\sigma_0}{\sqrt{g_*}}. \tag{3.59}$$

We have used M_{Pl} to denote the Planck mass, g_{*s}, g_* to denote the relativistic degrees of freedom associated with the entropy and energy density, respectively, and

44
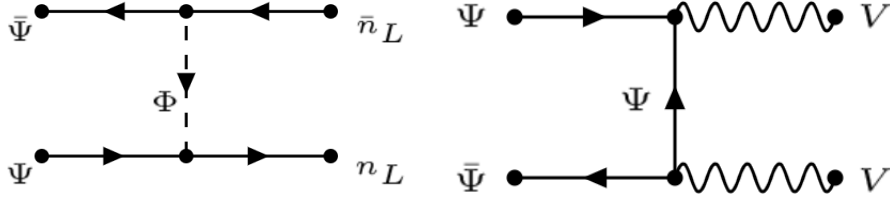
Figure 3.3: t-channel Ψ decays to nn and VV.

$$x_f = \frac{m_\Psi}{T_f} = \ln\left(0.076 m_\Psi \xi\right) - \frac{1}{2}\ln\left[\ln\left(0.076 m_\Psi \xi\right)\right], \tag{3.60}$$

with T_f being the freeze-out temperature. Comparing this expression for Ω_Ψ with the result from CMB data obtained by the Planck experiment:

$$\Omega_{Planck} h^2 = 0.1186 \pm 0.006 \ \ (3\sigma). \tag{3.61}$$

The case where $\mathcal{S} = 0$ (the no mixing limit) is excluded by this constraint. We also note that a sufficiently large value of g will lead to DM under-abundane.

3.9 Numerical Results

The model as detailed has ten parameters of interest: z (3), m_N, m_Ψ, m_Φ, λ_x (4) and $\mathcal{S}$ (3). For simplicity we have assumed that the z are real and that the N are degenerate. We consider the region of parameter space given by

45

Figure 3.4: Projections of the allowed parameter region, (a) in the $m_\Psi - m_\Phi$ plane, (b) the $\lambda_\chi - m_\Phi$ plane, (c) in the $m_\Psi - \langle z \rangle$ plane (where $\langle z \rangle = |z|/\sqrt{3}$), and (d)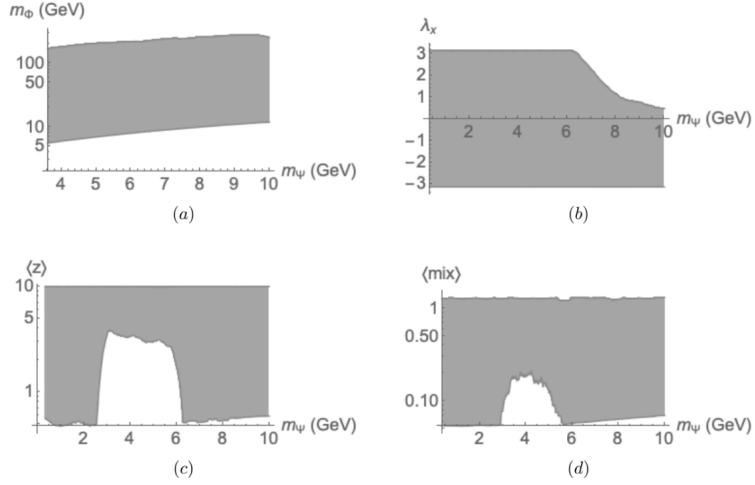 in the $m_\Psi - \langle mix \rangle$ plane, where $\langle mix \rangle$ is defined in eq (112). The unevenness in the curves are due to numerical inaccuracies.

$$0.5\text{GeV} \leq m_\Psi \leq 10\text{GeV}, \quad \min\{1.1m_\Psi,\, m_\Psi + 2\text{GeV}\} \leq m_\Phi < 500\text{GeV}, \tag{3.62}$$

$$2\text{GeV} \leq m_N \leq 1.5\text{TeV}, \quad |\lambda_x| \leq \pi, \quad |\mathcal{S}_i| < 1, \quad |z_i|^2 \leq 10 \ \ (i = 1,\, 2,\, 3). \tag{3.63}$$

A full scan over this region would be cumbersome and prohibitively time-consuming. Instead, we use a publicly-available optimization package [22] to obtain the allowed parameter space, given by the constrains above. We visualize the projections in the $m_\Psi - m_\Phi$ plane, the $m_\Psi - \langle z \rangle = |z|/\sqrt{3}$ plane, and the $m_\Psi - \langle mix \rangle$ plane, where

$$\langle mix \rangle = \sum |z_i|^2 \mathcal{S}_i^2 \tag{3.64}$$

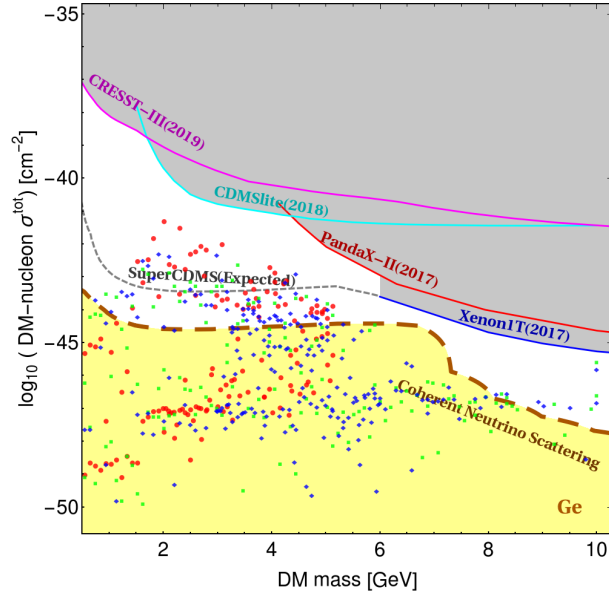and the results are given in (fig. 3.4). These projections show the constrains of interest; other

46

Figure 3.5: Experimental limits on the direct detection cross section σ. The upper curves are obtained, from left to right, from the CRESST, CDMS, PandaX and Xenon1T experiments, and the expected sensitivity limit for the superCDMS experiment; the coherent neutrino scattering regions are calculated for Xe (left) and Ge (right). For illustration we also include the cross sections corresponding to a selection of points on the boundary of the allowed region of parameter space, on the upper and lower boundaries of Fig. ()(a) (green points), of Fig. ()(c) (red points), and of Fig. ()(d) (blue points).

planes (ie $m_\Psi - m_N$, and $m_\Psi - \lambda_x$) reveal that the full region within the above constraints is allowed and satisfied by some combination of the other parameters.

In Fig. 3.5 we plot the values of the direct-detection cross sections for a selection of points on or close to the boundary of the allowed region of parameter space. The points are chosen only to illustrate that there is a region of parameter space within the sensitivity reach of SuperCDMS, but that this experiment cannot exclude the model; it is also worth noting that a (different) region of parameter space will correspond to cross sections above the coherent neutrino scattering 'floor'. Both these regions are significant in size: restricting the model to either (or both) would not require fine tuning.

Chapter 4

Conclusions

In this thesis, we have considered two separate models of dark matter, both of which include some minor extensions to the Standard Model in the form of a dark sector, which interacts with itself. In the first model, the dark sector consists of a complex scalar with an exact dark $U(1)$ symmetry. We investigated the possibility of a Bose einstein condensate forming in association with this precisely conserved charge and showed that, at sufficiently early times, the self-interaction among the scalar particles provides a repulsive force to balance the increasing early-universe density of the gas. In other words, in the absence of a self-interaction ($\lambda_\chi = 0$), there will always be a condensate at sufficiently early times in the universe. However, when a self-interaction is introduced, a condensate will only form if the charge per unit entropy is above a m_χ and λ_χ dependent minimum. At present times, we showed that a condensate will only persist if the dark matter mass is within the pico-eV range.

The direct-detection limits on this model are restrictive, allowing only small ϵ

and/or small m_χ (fig. 2.4). Even so, this range is extended from the traditional Higgs-portal model [7, 6] due to the existence of a chemical potential, which can be adjusted to satisfy the relic abundance constraints. We do not discuss indirect detection constraints, as these will be the same as the case of the usual Higgs-portal models.

The second model we have considered is more complex and introduces a more varied dark sector, consisting of a massive scalar Φ, two near-degenerate fermions $\Psi_{1,2}$, which interact strongly via a $U(1)_{dark}$ symmetry and associated gauge boson V. The fermions, $\Psi_{1,2}$ have opposite $U(1)_{dark}$ charge and serve as the dark matter candidates for this model. We have also introduced a (softly broken) $\mathbb{Z}_2$ symmetry to suppress mixing of the V with SM photons but still allow the V to decay into neutrinos. The lifetime for this decay is short enough so as not to interfere with relic abundance, LSS formation, or core v cusp limits. This model is a modification of a previously considered model, and it preserves the naturally small DM-SM interaction cross sections.

Experimental limits on the direct-detection cross section come from core v. cusp data provide restrictions on the strong coupling and m_V. We acquire an upper bound, $m_\Psi \lesssim 10\text{GeV}$, on the dark matter mass due to out requirement that Ψ_1 and Ψ_2 do not form bound states, since this would produce screened interactions and, therefore, difficulties satisfying the core v. cusp limits. Though the bound state issue might also be circumvented by requiring that the dark matter temperature is above the ionization energy of the Ψ_1 and Ψ_2 bound states, we do not do this because any such temperature effects will be masked by the large uncertainties in the cross section limits.

The DM-nucleon cross section in this model is a one-loop process and therefore

naturally suppressed. Thus, direct-detection does not provide strong limits on this model. Furthermore, the data on neutrino oscillations is not precise enough to produce significant restrictions; similarly, the limits from muon anomalous magnetic moment do not constrain our parameter space further. The most distinct direct-detection signature would thus come from the $\Psi_i\Psi_i \to \nu\nu$ process, which would produce a monochromatic neutrino line from both the sun and galactic halo. However, current experiments do not possess the sensitivity to detect such a signal.

Bibliography

[1] H. Babcock. The roation of the andromeda neblua. *Lick Observatory bulletin; no. 498. Berkeley : University of California Press*, 1939.

[2] ML Bellac. *Thermal Field Theory*. Cambridge University Press, 2000.

[3] M Carena and A Gouvea et al. Invisible z-boson decays at e+e- colliders. *Phys. Rev. D 68, 113007*, 2003.

[4] Douglas Clowe and Marusa Bradac et al. A direct empirical proof of the existence of dark matter. *Astrophys.J.648:L109-L113*, 2006.

[5] Sally Dawson and Howard E. Haber. A primer on higgs boson low-energy theorems. In *C89-01-02 (Bombay HEP Workshop 1989:0324-345), p.0324-345 SCIPP-89/14*, 1989.

[6] R Agnese et al. (SuperCDMS Collaboration). Low-mass dark matter search with cdmslite. *Phys. Rev. D 97, 022002*, 2018.

[7] E. Aprile et al. (XENON Collaboration). First dark matter search results from the xenon1t experiment. *Phys. Rev. Lett. 119, 181301*, 2017.

[8] A. Liam Fitzpatricka and Wick Haxton et al. The effective field theory of dark matter direct detection. *Journal of Cosmology and Astroparticle Physics, Volume 2013*, 2013.

[9] W Forman and C Jones et al. Hot cornoae around early-type galaxies. *The Astrophysical Jounal, 293: 102-119*, 1974.

[10] Vannia GonzÃ¡lez-MacÃas and JosÃ© I. Illana et al. A realistic model for dark matter interactions in the neutrino portal paradigm. *J. J. High Energ. Phys. (2016) 2016: 171*, 2016.

[11] Howard E. Haber and H. Arthur Weldon. Finite-temperature symmetry breaking as bose-einstein condensation. *Phys. Rev. D 25, 502*, 1982.

[12] E Hubble. Angular rotations of spiral nebulae. *Astrophysical Journal, vol. 81, p.334*, 1935.

[13] Gerard Jungman and Marc Kamionkowski et al. Supersymmetric dark matter. *Phys.Rept. 267, 195-373*, 1996.

[14] J. I. Kapusta and C. Gale. *Finite-Temperature Field Theory: Principles and Applications*. Cambridge University Press, 2011.

[15] JI Kapusta. Bose-einstein condensation, spontaneous symmetry breaking, and gauge theories. *Phys. Rev. D 24*, 1981.

[16] M Kawasaki and K Kohri et al. Revisiting big-bang nucleosynthesis constraints on dark-matter annihilation. *Physics Letters B, Volume 751*, 2015.

[17] EW Kolb and MS Turner. *The Early Universe*. CRC Press, 1990.

[18] Jacques P. Leveille. The second-order weak correction to (g - 2) of the muon in arbitrary gauge models. *Nuclear Physics, Section B, Volume 137, Issue 1, p. 63-76.*, 1978.

[19] S Nesseris M Kunz and I Sawicki. Constraints on dark-matter properties from large-scale structure. *Phys. Rev. D 94, 023510*, 2016.

[20] Adriaan Van Maanen. Adriaan van maanen on the significance of internal motions in spiral nebulae. *Journal for the History of Astronomy, Vol. 5, p.52*, 1974.

[21] Carlo Nipoti and James Binney. Early flattening of dark matter cusps in dwarf spheroidal galaxies. *Monthly Notices of the Royal Astronomical Society, Volume 446, Issue 2, 11*, 2015.

[22] NLOPT. https://nlopt.readthedocs.io/en/latest/. 2019.

[23] JP Ostriker and PJE Peebles et al. The size and mass of galaxies and the mass of the universe. *The Astrophysical Journal, 193: L1-L4*, 1974.

[24] R. K. Pathria and P. D. Beale. *Statistical Mechanics*. Academic Press, 2011.

[25] MS Roberts and RN Whitehurst. The rotation curve and geometry of m31 at large galactocentric distances. *The Astropysical Journal, 201: 327-346*, 1975.

[26] Vera C. Rubin and W. Kent Ford. Rotation of the andromeda nebula from a spectroscopic survey of emission regions. *The Astrophysical Journal, Vol. 159*, 1970.

[27] MA Shifman and AI Vainshtein et al. Remarks on higgs boson interactions with nucleons. *Phys. Lett. 78B, 443*, 1978.

[28] S. Smith. he mass of the virgo cluster. *Astrophysical Journal, vol. 83, p.23*, 1936.

[29] Sean Tulin and Hai-Bo Yu. Dark matter self-interactions and small scale structure. *Physics Reports*, 2018.

[30] F. Zwicky. The redshift of extragalactic nebulae. *Helvetica Physica Acta*, 1933.

Appendix A

Appendix

A.1 Thermodynamics of a Bose Gas

The Lagrangian for dark Bose gase (excluding interactions with the Standard Model) is given by

$$\mathcal{L} = |\partial\chi|^2 - m^2|\chi|^2 - \frac{1}{2}\lambda_\chi|\chi|^4. \tag{A.1}$$

As usual, we write the complex field χ as $\chi = (A_1 + iA_2)/\sqrt{2}$, so that the Hamiltonian and total conserved charge Q_{be} are

$$H = \int d^3x \left[\frac{1}{2}\boldsymbol{\pi}^2 + \frac{1}{2}|\nabla\boldsymbol{A}|^2 + V\right], \quad Q_{be} = -\int d^3x(A_1\pi_2 - A_2\pi_1), \tag{A.2}$$

where π_i is the canonical momentum conjugate to A_i.

If a condensate is to form then $A_1 \to A_1 + C$. We lose no generality in making this substitution; in the absence of a condensate we will simply have $C \to 0$. Then we use

the Matsubara formalism of finite-temperature field theory [14] and obtain the pressure as given by [15, 11]

$$P_{be} = \frac{\mu^2 - m_\chi^2}{2} C^2 + \frac{2}{3} \int d\tilde{\boldsymbol{p}}\, p^2 \mathcal{F}_+ + \frac{1}{8}\lambda_\chi C^4 - \lambda_\chi \left(\frac{1}{2}C^2 + \int d\tilde{\boldsymbol{p}}\mathcal{F}_+ \right)^2 + \mathcal{O}(\lambda_\chi^2), \quad \text{(A.3)}$$

to $\mathcal{O}(\lambda_\chi)$, where we have used

$$\mathcal{F}_\pm = \frac{1}{e^{\beta(E-\mu)} - 1} \pm \frac{1}{e^{\beta(E+\mu)} - 1}; \quad \bar{\mathcal{F}}_\pm = \mathcal{F}_\pm|_{\mu=m_\chi}, \quad \text{(A.4)}$$

$$d\tilde{\boldsymbol{p}} = \frac{d^3\boldsymbol{p}}{(2\pi)^3 2E}; \quad E = \sqrt{\boldsymbol{p}^2 + m_\chi^2}. \quad \text{(A.5)}$$

The Standard Model coupling, $\epsilon|\phi|^2|\chi|^2$, which we have thus far neglected, will introduce and additional contribution

$$\Delta P_{be} = -\epsilon F_H \left(\frac{1}{2}C^2 + \int d\tilde{\boldsymbol{p}}\mathcal{F}_+ \right); \quad F_H = \frac{m_H^2}{\pi^2} \int_0^\infty d\alpha \frac{\sinh^2\alpha}{e^{(m_H/T)\cosh\alpha} - 1}, \quad \text{(A.6)}$$

where F_H comes from the ϕsymmetry breaking $F_H \to v^2 + F_H/4$. When $m_H > m_\chi$, as we assume for this paper, this term is subdominant.

Before proceeding we remark on the type of perturbative expansion we will use: we assume that C is independent of λ_χ, and μ to have a λ_χ dependence; we believe this to be reasonable because, for example, the condition for the presence of a BEc when $\lambda_\chi = 0$ is $\mu = m_\chi$, and becomes $\mu > m_\chi$ when $\lambda_{be} \neq 0$ (see below) that naturally leads to a relation of the form $\mu = m_\chi + \mathcal{O}(\lambda_\chi)$.

The zero-momentum component C is determined by the condition that it minimizes the thermodynamic potential $-P_{be}(C, \mu, T)$:

$$\frac{\partial P_{be}}{\partial C} = \lambda_\chi C \left\{ \delta - \mathbb{F} - \frac{1}{2}C^2 \right\} + \mathcal{O}(\lambda_\chi^2), \tag{A.7}$$

where ($\bar{\mathcal{F}}_\pm$ are defined in (A.4))

$$\mu^2 = m_\chi^2 + \lambda_\chi \delta; \quad \mathbb{F} = 2 \int d\tilde{\boldsymbol{p}} \bar{\mathcal{F}}_+. \tag{A.8}$$

So there are two cases:

1. $\delta < \mathbb{F}$: then there's a single extremum, ,$C = 0$ which is a maximum and corresponds to the stable state; there is no BEc.

2. $\delta > \mathbb{F}$: then there are two extrema: $C = 0$ which is now a minimum, and does not correspond to the stable state, and

$$C^2 = 2(\delta - \mathbb{F}) + \mathcal{O}(\lambda_\chi), \tag{A.9}$$

which is a maximum and corresponds to the stable (BEc) configuration.

The transition occurs when $\delta = \mathbb{F}$; approximating $\mathbb{F} \simeq \mathbb{F}(m_\chi = 0)$ we find that the critical temperature is

$$T_C^2 \simeq \frac{6}{\lambda_\chi}(\mu^2 - m_\chi^2), \tag{A.10}$$

which is a known result [15, 11].

From P_{be} we find the expressions for the charge density q_{be} and entropy density s_{be} to $\mathcal{O}(\lambda_\chi)$:

- $\delta < \mathbb{F}$:

$$P_{be} = \frac{2}{3} \int d\tilde{\boldsymbol{p}} p^2 \mathcal{F}_+ - \lambda_\chi \left(\int d\tilde{\boldsymbol{p}} \mathcal{F}_+ \right)^2 \tag{A.11}$$

$$q_{be} = \int \frac{d^3\boldsymbol{p}}{(2\pi)^3} \bar{\mathcal{F}}_- + \frac{4\lambda_\chi \mathbb{F}}{m} \left(\frac{m}{4} \int \frac{d^3\boldsymbol{p}}{(2\pi)^3} \frac{\bar{\mathcal{F}}_+ - \bar{\mathcal{F}}_-}{p^2} + \int d\tilde{\boldsymbol{p}} \frac{E + m/2}{E + m} \bar{\mathcal{F}}_+ \right), \tag{A.12}$$

$$s_{be} = \int d_3\boldsymbol{p} \left(1 - \lambda_{be} \frac{2\mathbb{F}}{p^2} \right) \sum_{\pm} \left[(n_{be}^\pm + 1) \ln (n_{be}^\pm + 1) - n_{be}^\pm \ln n_\chi^\pm \right]_{\mu = m_\chi} \tag{A.13}$$

where $K^2 = 4 \int d\tilde{\boldsymbol{p}} \mathcal{F}_+$.

- $\delta = \mathbb{F}$:

$$P_{be} = \frac{2}{3} \int d\tilde{p}\, p^2 \bar{\mathcal{F}}_+ - \frac{1}{4} \lambda_\chi \mathbb{F} \left(\mathbb{F} - \frac{2}{m} \int d_3\boldsymbol{p} \bar{\mathcal{F}}_- \right), \tag{A.14}$$

$$q_{be} = \int \frac{d^3\boldsymbol{p}}{(2\pi)^3} \bar{\mathcal{F}}_- + \frac{4\lambda_\chi \mathbb{F}}{m} \left(\frac{m}{4} \int \frac{d^3\boldsymbol{p}}{(2\pi)^3} \frac{\bar{\mathcal{F}}_+ - \bar{\mathcal{F}}_-}{p^2} + \int d\tilde{\boldsymbol{p}} \frac{E + m/2}{E + m} \bar{F}_+ \right), \tag{A.15}$$

$$\begin{aligned} s_{be} = &\int d_3\boldsymbol{p} \left(1 - \lambda_\chi \frac{2\mathbb{F}}{p^2} \right) \sum_{\pm} \left[(n_{be}^\pm + 1) \ln (n_{be}^\pm + 1) - n_{be}^\pm \ln n_{be}^\pm \right]_{\mu = m_\chi} \\ &+ \frac{\lambda_{be} \mathbb{F}}{T} \int d\tilde{p} \left\{ \frac{E^2 + p^2}{p^2} (\bar{\mathcal{F}}_- - \bar{\mathcal{F}}_+) + \frac{3E^2 + mE - m^2}{m(E + m)} \bar{\mathcal{F}}_- \right\}. \end{aligned} \tag{A.16}$$

- $\delta > \mathbb{F}$:

$$P_{be} = \frac{2}{3} \int d\tilde{p} p^2 \bar{\mathcal{F}}_+ - \frac{1}{4} \lambda_\chi \left[\mathbb{F}^2 - \frac{C^4}{2} - \frac{C^2 + 2\mathbb{F}}{m} \int d_3\boldsymbol{p} \bar{\mathcal{F}}_- \right], \tag{A.17}$$

$$q_{be} = q_{be}^{(c)} + \int \frac{d^3\boldsymbol{p}}{(2\pi)^3} \bar{\mathcal{F}}_- + \mathcal{O}(\lambda_\chi), \tag{A.18}$$

$$\begin{aligned} s_{be} = &\int d_3\boldsymbol{p} \left(1 - \lambda_\chi \frac{2 \left(C^2 + \mathbb{F} \right)}{p^2} \right) \sum_{\pm} \left[(n_{be}^\pm + 1) \ln (n_{be}^\pm + 1) - n_{be}^\pm \ln n_{be}^\pm \right]_{\mu = m_\chi} \\ &+ \frac{\lambda_\chi \left(\mathbb{F} + C^2/2 \right)}{T} \int d\tilde{p} \left\{ \frac{E^2 + p^2}{p^2} (\bar{\mathcal{F}}_- - \bar{F}_+) + \frac{3E^2 + mE - m^2}{m(E + m)} \bar{\mathcal{F}}_- \right\}. \end{aligned} \tag{A.19}$$

with $q_{be}^{(c)} = m_{be} C^2 + \mathcal{O}(\lambda_\chi)$. The $\mathcal{O}(\lambda_\chi)$ corrections to q_{be} in the BEc phase are obtained from the $\mathcal{O}(\lambda_{be}^2)$ terms in P_{be}, fortunately these are not needed.
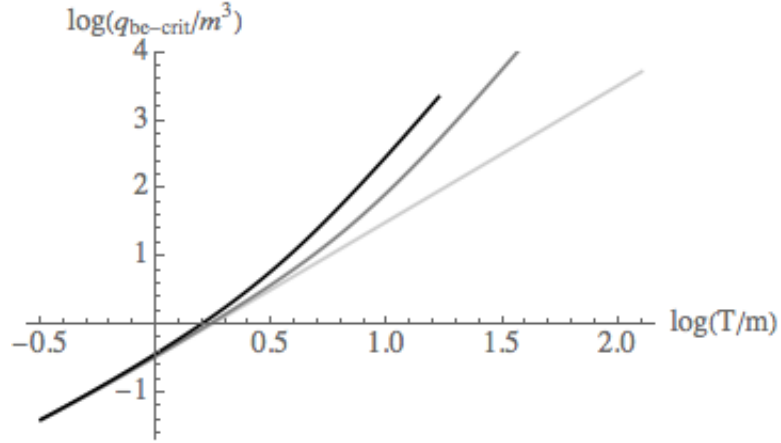
Figure A.1: Plot of the critical density function of T for $\lambda_\chi = 0$ (light gray), 0.1, (dark gray), and 0.5 (black).

The curvature of the thermodynamic potential $-P_{be}(C, \mu, T)$ at $C = 0$ equals $\lambda_\chi(\mathbb{F} - \delta) \simeq \lambda_\chi T^2/6 + m_\chi^2 - \mu^2$ for large T (see eqn (refeq:20)). In this regime the radiative corrections oppose the formation of a condensate; if this is indicative of the exact result, the condensate will disappear as $T \to \infty$. The behavior of the critical density (q_{be} at the transition) is given in fig. A.1 which also illustrates the effects of the $\mathcal{O}(\lambda_\chi T^2)$ contributions.

When the volume V is constant and the total charge in the system is Q_{be} the behavior of the condensate as a function of T can be obtained using standard arguments; the results are illustrated in fig. A.2 where the critical temperature T_C is defined by requiring $q_{be} = Q_{be}/V$ when $\delta = \mathbb{F}$.

In the non-relativistic limit ($x \gg 1$) the $\mathcal{O}(\lambda_\chi)$ can be ignored in the phase where there is no condensate. To see this, consider, for example the expression for P_{be}:

$$P_{be} = \frac{m_\chi^4}{\pi^2 x^2}\left[\cosh(\beta\mu)K_2(x) + \frac{\cosh(2\beta\mu)}{4}K_2(2x) - \frac{\lambda_{be}\cosh^2(\beta\mu)}{4\pi^2}K_1^2(x) + ...\right], \quad (A.20)$$
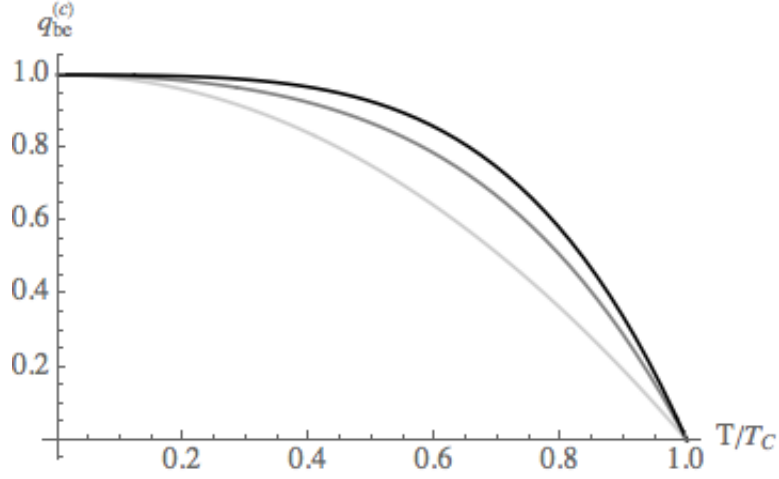
57

Figure A.2: Plot of the condensate density $q_{be}^{(c)}$ as a function of T for constant volume and $\lambda_\chi = 0$ (light gray), 0.1 (dark gray), and 0.5 (black), when the critical temperature (see text) $T_C = 10m_\chi$. When $T_C \ll m_\chi$ the $\mathcal{O}(\lambda_\chi)$ effects are negligible.

which shows that the leading $\mathcal{O}(\lambda_\chi)$ corrections are smaller than the subdominant $\mathcal{O}(\lambda_\chi^0)$ contributions. This behavior is reproduced in all thermodynamic quantities in when $x \gg 1$ and there is no BEc.

We also need the behavior of the thermodynamic quantities at the transition (when $\delta = \mathbb{F}$) in the ultra-relativistic ($x \ll 1$) and non-relativistic ($x \gg 1$) limits:

$$x \ll 1: \quad P_{be} = \frac{\pi^2 m_\chi^4}{45x^4}\left[1 + \frac{15\lambda_\chi}{16\pi^2}\right] + ...$$

$$q_{be} = \frac{m_\chi^3}{3x^2}\left[1 - \frac{3x}{\pi^2} + \frac{\lambda_\chi}{12x^2}\left(1 - \frac{3}{\pi^2}x\ln x\right) + ...\right]$$

$$s_{be} = \frac{4\pi^2 m_\chi^3}{45x^3}\left[1 + \frac{5\lambda_\chi}{16\pi^2}\right] + ...$$

$$\rho_{be} = \frac{\pi^2 m_\chi^4}{15x^4}\left[1 + \frac{5\lambda_\chi}{16\pi^2}\right] + ...$$

$$x \gg 1: \quad P_{be} = \frac{m_\chi^4 \zeta_{5/2}}{(2\pi)^{3/2}x^{5/2}}\left[1 + \frac{\zeta_{7/2}}{\zeta_{5/2}}\frac{15}{8x} + ...\right] + \lambda_\chi\frac{m_\chi^4 \zeta_{3/2}^2}{(2\pi x)^3} + ...$$

$$q_{be} = \frac{m_{be}^3 \zeta_{3/2}}{(2\pi x)^{3/2}}\left[1 + \frac{\zeta_{5/2}}{\zeta_{3/2}}\frac{15}{8x} + ...\right] + \frac{3\lambda_\chi m_\chi^3 \zeta_{3/2}^2}{2(2\pi x)^3} + ...$$

58

$$s_{be} = \frac{5m_\chi^3 \zeta_{5/2}}{2(2\pi x)^{3/2}} \left[1 + \frac{\zeta_{7/2}}{\zeta_{5/2}} \frac{21}{8x} + ... \right] + \frac{9\lambda_\chi m_\chi^3 \zeta_{3/2} \zeta_{5/2}}{128\pi^3 x^3} + ...$$

$$\rho_{be} = \frac{m_{be}^4 \zeta_{3/2}}{(2\pi x)^{3/2}} \left[1 + \frac{\zeta_{5/2}}{\zeta_{3/2}} \frac{27}{8x} + ... \right] + \frac{\lambda_\chi m_\chi^4 \zeta_{3/2}^2}{(2\pi x)^3} + ...$$

where ρ_{be} is the energy density.

In particular, for small x,

$$x_{min} = \sqrt{\frac{\lambda_\chi}{12}} + \frac{3\lambda_\chi}{8\pi^2} + ... \tag{A.21}$$

The above minimum occurs when the $\mathcal{O}(\lambda_\chi)$ corrections to q_{be} are of the same size as the $\mathcal{O}(\lambda_\chi^0)$ contributions, so the validity of the expressions for such values of x should be examined. The leading expression for q_{be} is $\propto \int d^3\boldsymbol{p} \bar{\mathcal{F}}_-$ and behaves as x^{-2}, instead of x^{-3} as might be expected on dimensional grounds; such a suppression is not present in the $\mathcal{O}(\lambda_\chi)$ corrections. We argue that a reasonable estimate of the region where perturbation theory is valid is obtained by comparing the $\mathcal{O}(\lambda_\chi)$ corrections to q_{be} with a quantity that does not exhibit the above suppression, such as $\int d^3\boldsymbol{p} \bar{F}_+$. Using this we obtain

$$\int \frac{d^3\boldsymbol{p}}{(2\pi)^3} \bar{F}_+ > \frac{m_\chi^3 \lambda_\chi}{36x^4} \left(1 - \frac{3}{\pi^2} x\ln x + ... \right) \Rightarrow \frac{x}{1 - (3/\pi^2)x\ln x} > \frac{\lambda_\chi}{8.8} \tag{A.22}$$

as specifying the lowest value of x for which our perturbative expressions are trustworthy. Since $x_{\texttt{min}}$ satisfies this condition, the expression for q_{be}/s_{be} can be trusted near the minimum.

A.1.1 χ Propogator

The finite-temperature real-time formalism can be used to derive the Feynman rules and propogator from the above Hamiltonian and total charge operators. We define, as per the conventions of LeBellac [2]

$$D_{ij}^{>}(x - x') = \langle A_i(x)A_j(x') \rangle_\beta, \quad D_{ij}^{<}(x - x') = \langle A_j(x')A_i(x) \rangle_\beta, \quad \text{(A.23)}$$

where

$$\langle ... \rangle_\beta = \frac{tr\left\{ e^{-\beta H}... \right\}}{tr\left\{ e^{-\beta H} \right\}}. \quad \text{(A.24)}$$

Then if,

$$\rho_{ij}(k) = D_{ij}^{>}(k) - D_{ij}^{<}(k); \quad D_{ij}^{\gtrless}(k) = \int d^4x \, e^{+ik\cdot x} D_{ij}^{\gtrless}(x), \quad \text{(A.25)}$$

we have

$$D_{ij}^{<}(k) = f(k_0)\rho_{ij}(k), \quad D_{ij}^{>}(k) = -f(-k_0)\rho_{ij}(k); \quad f(k_0) = \left(e^{k_0\beta} - 1 \right)^{-1}. \quad \text{(A.26)}$$

From which we can calculate

$$\rho(k) = 2\pi\epsilon(k_0) \left[\frac{\delta(\omega^2 - \Omega_+^2) - \delta(\omega^2 - \Omega_-^2)}{\Omega_+^2 - \Omega_-^2} \right] \mathbb{R}(k), \quad \text{(A.27)}$$

$$\mathbb{R}(k) = \begin{pmatrix} k^2 + \mu - m^2 - \lambda_\chi C^2/2 & -2i\mu k_0 \\ 2i\mu k_0 & k^2 + \mu^2 - m^2 - 3\lambda_\chi C^2/2 \end{pmatrix}. \quad \text{(A.28)}$$

When $\mu = 0$, this reduces to the expected form. For this paper we will only need expressions with precision up to $\mathcal{O}(\lambda_\chi)$:

$$\rho(k)|_{\lambda_\chi=0} = \pi \sum_{s=\pm 1} (\mathbf{1} \pm \tau_2)\epsilon(k_0 \mp \mu)\delta((k_0 \mp \mu)^2 - \bar{E}_{\mathbf{k}}^2), \quad \text{(A.29)}$$

60

where $\bar{E}_{\mathbf{k}} = \sqrt{m_\chi^2 + \mathbf{k}^2}$. This expression will be valid in the presence or absence of a condenate, when $\mu = m_\chi$ or otherwise.

During the period when the SM and the Bose gas are in thermal equilibrium, we must consider the resonant contribution, which can occur for $m_H = 2m_{be}$. To account for this, we make the following substitution in $D_H^{\gtrless}$

$$2\pi\delta(p^2 - m_H^2) \to \frac{2\Gamma_H m_H}{(p^2 - m_H^2)^2 + (\Gamma_H m_H)^2}, \tag{A.30}$$

where Γ_H is the Higgs width.

A.1.2 Evaluation of G

In the presence of a condensate we write $\chi = [(A_1 + C) + iA_2]/\sqrt{2}$, where $A_{1,2}$ denote the fields and C the condensate amplitude. We also assume that decoupling occurs below the electroweak phase transition so that $|\phi|^2 = (v+h)^2/2$, where v is the SM vacuum expectation value, and h the Higgs field. We find, after an appropriate renormalization,

$$G_{BEc} = \left[v^2 C^2 G_{2-2} + \frac{1}{4}C^2 G_{2-4} + \frac{1}{4}v^2 G_{4-2} + \frac{1}{16}G_{4-4} \right]_{\mu=m_\chi}, \tag{A.31}$$

where

$$G_{2-2} = \int_0^\beta ds \int_0^\infty dt \int d^3\mathbf{x} \langle A_1(-is,\mathbf{x})\frac{dA_1(t,\mathbf{z})}{dt}\rangle\langle h(-is,\mathbf{x})\frac{dh(t,\mathbf{z})}{dt}\rangle, \tag{A.32}$$

$$G_{2-4} = \int_0^\beta ds \int_0^\infty dt \int d^3\mathbf{x} \langle A_1(-is,\mathbf{x})\frac{dA_1(t,\mathbf{z})}{dt}\rangle\langle h^2(-is,\mathbf{x})\frac{dh^2(t,\mathbf{z})}{dt}\rangle, \tag{A.33}$$

$$G_{4-2} = \int_0^\beta ds \int_0^\infty dt \int d^3\mathbf{x} \langle \mathbf{A}^2(-is,\mathbf{x})\frac{d\mathbf{A}^2(t,\mathbf{z})}{dt}\rangle\langle h(-is,\mathbf{x})\frac{dh(t,\mathbf{z})}{dt}\rangle, \tag{A.34}$$

$$G_{4-4} = \int_0^\beta ds \int_0^\infty dt \int d^3\mathbf{x} \langle \mathbf{A}^2(-is,\mathbf{x})\frac{d\mathbf{A}^2(t,\mathbf{z})}{dt}\rangle\langle h^2(-is,\mathbf{x})\frac{dh^2(t,\mathbf{z})}{dt}\rangle. \tag{A.35}$$

In the absence of a condensate we have

$$G_{BEc} = \frac{1}{4}v^2 G_{4-2} + \frac{1}{16}G_{4-4}\,, \tag{A.36}$$

(G_{BEc} denotes the expression for G in the absence of a condensate) evaluated at a chemical

potential $|\mu| < m_\chi$.

We evaluate the G_{n-m} using the standard Feynman rules for the real-time formalism

of finite-temperature field theory and the propagators derived above. The calculation is

straightforward but tedious; to simplify the expressions we use the following shortcuts:

$$E = E_{\mathbf{k}}, \qquad E' = E_{\mathbf{k}'}, \qquad \bar{E} = \bar{E}_{\mathbf{q}}, \qquad \bar{E}' = \bar{E}_{\mathbf{q}'},$$
$$n_H = n_H(E_{\mathbf{k}}), \quad n'_H = n_H(E_{\mathbf{k}'}), \quad n_{be}^\pm = n_{be}^\pm(\bar{E}_{\mathbf{q}}), \quad n_{be}^\pm{}' = n_{be}^\pm(\bar{E}_{\mathbf{q}'}), \tag{A.37}$$

and

$$d\tilde{\mathbf{k}} = \frac{d^3\mathbf{k}}{2E_{\mathbf{k}}(2\pi)^3}\,, \quad d\tilde{\mathbf{q}} = \frac{d^3\mathbf{q}}{2\bar{E}_{\mathbf{q}}(2\pi)^3}\,; \tag{A.38}$$

where

$$E_{\mathbf{k}} = \sqrt{m_H^2 + \mathbf{k}^2}\,, \quad \bar{E}_{\mathbf{q}} = \sqrt{m_\chi^2 + \mathbf{q}^2}\,; \quad n_{be}^{(\pm)}(\bar{E}) = \left[e^{\beta(\bar{E}\mp\mu)} - 1\right]^{-1}\,, \tag{A.39}$$

and m_H denotes the Higgs mass.

Then the G_{n-m} (for arbitrary μ) are given by

- G_{4-4}

  - $G_{4-4} = 16\pi\beta \int d\tilde{k}d\tilde{k}'d\tilde{q}d\tilde{q}'(2\pi)^3\,\delta^{(3)}(\mathbf{k} + \mathbf{k}' + \mathbf{q} + \mathbf{q}')\mathcal{G}_{4-4}\,;$

  - $\mathcal{G}_{4-4} = \frac{1}{2}(1 + n_{\mathbf{t}H})(1 + n'_{\mathbf{t}H})n_{\mathbf{t}be}^+ n_{\mathbf{t}be}^-{}'\,\delta(E + E' - \bar{E} - \bar{E}')\,(E + E')^2$

  - $\quad + \frac{1}{2}(1 + n_{\mathbf{t}be}^+)(1 + n_{\mathbf{t}be}^-{}')n_{\mathbf{t}H}n'_{\mathbf{t}H}\,\delta(E + E' - \bar{E} - \bar{E}')\,(E + E')^2$

  - $\quad + (1 + n_{\mathbf{t}H})(1 + n_{\mathbf{t}be}^+)n'_{\mathbf{t}H}n_{\mathbf{t}be}^+{}'\,\delta(E + \bar{E} - E' - \bar{E}')\,(E - E')^2$

$$- \quad +(1+n_{\mathbf{t}H})(1+n_{\mathbf{tbe}}^-)n'_{\mathbf{t}H}n_{\mathbf{tbe}'}^-\delta(E+\bar{E}-E'-\bar{E}')\,(E-E')^2\,,$$

where the 4 terms represent the processes $hh \leftrightarrow \chi\chi^\dagger$, $h\chi \to h\chi$, and $h\chi^\dagger \to h\chi^\dagger$ respectively; the factors of $1/2$ are due to Bose statistics.

- G_{2-4}

  - $G_{2-4} = 2\pi\beta \int d\tilde{k}d\tilde{k}'d\tilde{q}(2\pi)^3\delta^{(3)}(\mathbf{k}+\mathbf{k}'+\mathbf{q})\mathcal{G}_{2-4}\,;$

  - $\mathcal{G}_{2-4} = \frac{1}{2}(1+n_{\mathbf{t}H})\,(1+n'_{\mathbf{t}H})n_{\mathbf{tbe}}^-\,\delta(E+E'-\bar{E}-m_\chi)\,(E+E')^2$

  - $\quad +\frac{1}{2}(1+n_{\mathbf{tbe}}^-)n_{\mathbf{t}H}n'_{\mathbf{t}H}\,\delta(E+E'-\bar{E}-m_\chi)\,(E+E')^2$

  - $\quad +(1+n_{\mathbf{t}H})n'_{\mathbf{t}H}n_{\mathbf{tbe}}^+\,\delta(E+m_\chi-E'-\bar{E})\,(E-E')^2$

  - $\quad +(1+n_{\mathbf{t}H})(1+n_{\mathbf{tbe}}^+)n'_{\mathbf{t}H}\,\delta(E+\bar{E}-E'-m_\chi)\,(E-E')^2\,,$

these 4 terms represent the processes $hh \leftrightarrow C\chi^\dagger$ and $hC \leftrightarrow h\chi$, where C corresponds to a particle in the condensate (mass m_χ and zero momentum); the factors of $1/2$ are due to Bose statistics.

- G_{4-2}

  - $G_{2-4} = 4\pi\beta \int d\tilde{k}d\tilde{q}d\tilde{q}'(2\pi)^3\delta^{(3)}(\mathbf{k}+\mathbf{q}+\mathbf{q}')\mathcal{G}_{4-2}\,;$

  - $\mathcal{G}_{4-2} = \left[(1+n_{\mathbf{tbe}}^+)(1+n_{\mathbf{tbe}'}^-)n_{\mathbf{t}H} + (1+n_{\mathbf{t}H})\,n_{\mathbf{tbe}}^+\,n_{\mathbf{tbe}'}^-\right]E^2\delta(\bar{E}+\bar{E}'-E)\,,$

these 2 terms represent the processes $h \leftrightarrow \chi\chi^\dagger$.

- G_{2-2}

  - $G_{2-2} = \frac{1}{2}\pi\beta \int d\tilde{k}d\tilde{q}(2\pi)^3\delta^{(3)}(\mathbf{k}+\mathbf{q})\mathcal{G}_{2-2}\,;$

  - $\mathcal{G}_{2-2} = \left[(1+n_{\mathbf{t}H})n_{\mathbf{tbe}}^- + (1+n_{\mathbf{tbe}}^-)n_{\mathbf{t}H}(E)\right]E^2\delta(E-m_\chi-\bar{E})\,,$

63

these 2 terms represent the processes $h \leftrightarrow C\chi^{\dagger}$.

In the non-relativistic limit, where m_χ, $m_{\mathbf{t}H} \gg T$ we find[1]

$$G_{2-2}^{(NR)}\Big|_{\mu=m_\chi} \simeq \frac{m_{\mathbf{t}H}}{r\sqrt{(2\pi)^3 x}} \frac{2u_\Gamma\, e^{-2x}}{u_\Gamma^2 + (r^2 - 4)^2}\,; \qquad (A.40)$$

$$G_{2-4}^{(NR)}\Big|_{\mu=m_\chi} \simeq \left(\frac{m_{\mathbf{t}H}}{2\pi r x}\right)^3 \left[2r^2 x^2 \rho K_1(\rho) + \zeta_3\left(\frac{(r+1)^2}{4r}\right)\right] e^{-rx}\,; \qquad (A.41)$$

$$G_{4-2}^{(NR)} \simeq \left(\frac{m_H}{2\pi}\right)^3 \frac{4}{x^2 r^3} \left[e^{-rx}\sqrt{\pi\left(\frac{rx}{2}\right)^3 \left(\frac{r^2}{4} - 1\right)}\,\theta(r-2) + \frac{\mathrm{Li}_{3/2}(z)}{z}\frac{2u_\Gamma\, e^{-2x}}{u_\Gamma^2 + (r^2 - 4)^2}\right]\,; \qquad (A.42)$$

$$G_{4-4}^{(NR)} \simeq \frac{1}{16}\frac{m_H^5}{r^3(1+r)^{7/2}}\left(\frac{2}{\pi x}\right)^{9/2} e^{-rx}\left(z + \frac{1}{z}e^{-2x}\right)\,, \qquad (A.43)$$

where K_1, ζ_3 and Li denote the usual Bessel, zeta and Poly-logarithmic functions, and we defined

$$r = \frac{m_{\mathbf{t}H}}{m\,\,\chi}, \quad \rho = \frac{4r|r-1|x}{\sqrt{2(r^2+1)}}, \quad u_\Gamma = r^2\frac{\Gamma_{sm}}{m_{\mathbf{t}H}}, \quad z = e^{\beta(\mu-m_\chi)}\,. \qquad (A.44)$$

Before continuing it is worth pointing out a slight difference between the expression for Γ derived above and the corresponding expression usually found in the literature: the calculated Γ describes the energy transfer between the SM and the Bose gas, which leads to the $(E \pm E')^2$ factors. As a result Γ has a factor $\sim (\mathrm{mass}/T)^2$ compared to the usual expressions, which determine the change in the DM particle number. Because of this the

---

[1]$G_{2-2,\,2-4}$ contribute only when there is condensate, so we evaluate then them only for $\mu = m_\chi$; the expressions for $G_{4-2,\,4-4}$ are valid for all μ.

decoupling temperature will be somewhat higher than usual; this difference, however, is not significant given that the criterion is not sharply defined.